# Pre-print

Wittmann, H., Malusà, M. G., Resentini, A., Garzanti, E., & Niedermann, S. (2016).

The cosmogenic record of mountain erosion transmitted across a foreland basin: Source-to-sink analysis of in situ $^{10}$Be, $^{26}$Al and $^{21}$Ne in sediment of the Po river catchment.

Earth and Planetary Science Letters, 452, 258-271.

*http://dx.doi.org/10.1016/j.epsl.2016.07.017*

# The cosmogenic record of mountain erosion transmitted across a foreland basin: source-to-sink analysis of *in situ* $^{10}$Be, $^{26}$Al and $^{21}$Ne in sediment of the Po river catchment

Hella Wittmann[1*], Marco G. Malusà[2], Alberto Resentini[2], Eduardo Garzanti[2], Samuel Niedermann[1]

[1] Helmholtz Centre Potsdam, GFZ German Research Centre for Geosciences, Telegrafenberg, 14473 Potsdam, Germany
[2] Department of Earth and Environmental Sciences, University of Milano-Bicocca, Piazza della Scienza 4, 20126 Milan, Italy

*Corresponding author: phone: +49 331 288-2820; E-mail address: wittmann@gfz-potsdam.de

**ABSTRACT:** We analyze the source-to-sink variations of *in situ* $^{10}$Be, $^{26}$Al and $^{21}$Ne concentrations in modern sediment of the Po river catchment, from Alpine, Apennine, floodplain, and delta samples, in order to investigate how the cosmogenic record of orogenic erosion is transmitted across a fast-subsiding foreland basin. The *in situ* $^{10}$Be concentrations in the analyzed samples range from ~$0.8\times10^4$ at/$g_{QTZ}$ to ~$6.5\times10^4$ at/$g_{QTZ}$. The $^{10}$Be-derived denudation rates range from 0.1-1.5 mm/yr in the Alpine source areas and from 0.3-0.5 mm/yr in the Apenninic source areas. The highest $^{10}$Be-derived denudation rates are found in the western Central Alps (1.5 mm/yr). From these data, we constrain a sediment flux leaving the Alpine and the Apenninic source areas (>27 Mt/yr and ca. 5 Mt/yr, respectively) that is notably higher than the estimates of sediment export provided by gauging (~10 Mt/yr at the Po delta).

We observe a high variability in $^{10}$Be concentrations and $^{10}$Be-derived denudation rates in the source areas. In the Po Plain, little variability is observed, and at the same time, the area-weighted $^{10}$Be concentration of $(2.29\pm1.57)\times10^4$ at/$g_{QTZ}$ (±1SD of the dataset) from both the Alps and the Apennines is poorly modified (by tributary input) in sediment of the Po Plain ($(2.68\pm0.78, \pm1SD)\times10^4$ at/$g_{QTZ}$). The buffering effect of the Po floodplain largely removes scattered $^{10}$Be signals.

We test for several potential perturbations of the cosmogenic nuclide record during source to sink transfer in the Po basin. We find that sediment trapping in deep glacial lakes or behind dams does not significantly change the $^{10}$Be-mountain record. For example, similar $^{10}$Be concentrations are measured upstream and downstream of the postglacial Lake Maggiore, suggesting that denudation rates prior to lake formation were similar to today. On the scale of the entire basin, the $^{10}$Be concentration of basins with major dams is similar to those without major dams. A potential modification of the $^{10}$Be-mountain record during

sediment storage in the subsiding Po Plain can be excluded as measured $^{26}Al/^{10}Be$ ratios do not show the addition of deeply buried material. A barely resolvable excess $^{21}Ne$ signal in the Po plain indicates recycling of previously eroded sediment rather than accumulation of cosmogenic nuclides during surficial floodplain transport. Our results demonstrate that the cosmogenic record of mountain erosion is effectively transmitted from the source areas to the sediment sink, even across a strongly subsiding foreland basin. This record is poorly influenced by a range of potential geological and anthropogenic sources of bias, and is largely independent from upstream sediment interception and sediment storage in the floodplain.

**Keywords:** Cosmogenic nuclides; In-situ $^{10}Be/^{26}Al/^{21}Ne$; Po Plain; Alps; Apennines; Mountain erosion; Floodplain/basin subsidence, Source-to-sink, Signal transmittance

## 1. INTRODUCTION

Quantifying mountain erosion over different time scales is key to understanding how tectonics, climate, and human impact may shape our landscape (Kirchner et al., 2001; Cyr and Granger, 2008; Hidy et al, 2014). The depositional record can provide a powerful mirror of mountain erosion, but the routing of sediment through lowlands may modify or completely shred the original erosion signal (Jerolmack and Paola, 2010; Simpson and Castelltort, 2012; Armitage et al., 2013). As a consequence, an integrated approach insensitive to a range of potential sources of geological and anthropogenic bias is required in order to trace signals from upstream mountainous areas to the lowlands, so that sediment routing from the source to the floodplain sink can be quantified. A method capable of doing so is *in situ* cosmogenic nuclides (mainly $^{10}Be$) measured in river sand, which provides average denudation rates over time scales of $10^2$ to $10^5$ years, depending on the prevailing denudation rate in the source area (Lal, 1991; von Blanckenburg, 2005). This method has been recently extended to large lowland basins such as the Amazon (Wittmann et al., 2009; 2011a,b). The main finding of these works is that the concentrations of *in situ* $^{10}Be$ and $^{26}Al$ inherited during erosion processes in the sediment source area are largely unchanged during sediment storage and floodplain reworking of sediment, or the change can be corrected for, when using a paired nuclide approach of $^{26}Al/^{10}Be$. Thus, the method and its robustness with respect to sediment storage and reworking has been extensively

documented in the Amazon and Ganga basins (Wittmann and von Blanckenburg, 2009; Wittmann et al., 2009; 2011a,b; Lupker et al., 2012).

Given these recent advances of the method with respect to sediment storage, we can proceed with the application to a geologically complex, medium-size foreland basin of Alpine type, namely the Po river basin (~74,000 $km^2$), where the source-to-sink connectivity is disturbed by fast tectonic subsidence (Carminati and Di Donato, 1999), by sediment trapping in deep postglacial lakes (Hinderer, 2001), and by heavy human modifications through dam and reservoir construction (Syvitski and Kettner, 2007). The Po basin is well studied not only with respect to the geology of the source and sink areas (e.g., Garzanti et al., 2011; Ghielmi et al., 2013), but also with respect to modern (decadal-scale) sediment fluxes and their decline because of dams and reservoirs (Bartolini et al., 1996; Hinderer et al., 2013). Moreover, *in situ* $^{10}$Be-derived denudation rate data are already available in several subbasins (Wittmann et al., 2007; Norton et al., 2011).

In this study, we measure new *in situ* $^{10}$Be concentrations in sediments carried by the major Alpine and Apenninic tributaries draining into the Po Plain, and investigate the propagation of the $^{10}$Be cosmogenic signal from the source areas to the Po delta. We assess the influence of deep postglacial lakes, moraines and large dams on the $^{10}$Be concentrations. We use the $^{26}$Al/$^{10}$Be ratio to monitor the potential reworking of deeply buried sediments in the lowlands, and present stable $^{21}$Ne concentrations from the Alpine source to the delta. The long-term cosmogenic nuclide-derived sediment fluxes are then compared with the estimates of sediment flux based on gauging, and we discuss the potential causes of discrepancy between the two methods.

Using these multiple cosmogenic nuclide and sediment gauging tools, we highlight the robustness of *in situ* $^{10}$Be as a faithful tracer of mountain erosion and sediment transport, even in medium-sized floodplains such as the Po Plain where sediment input from source areas is potentially not as effectively buffered as in large floodplains like the Amazon or the Ganga.

## 2. STUDY AREA

The Po river drains a complex arcuate orogen developed along the Adria-Europe plate boundary on top of two interacting subduction zones, the Alpine subduction zone to the north and the Apenninic subduction zone to the south (Fig. 1) (Handy et al., 2010; Malusà et al., 2015, and references therein). On the northern side of the drainage, the Central and Eastern Alps include the Southalpine and Austroalpine units, derived from the Adriatic paleomargin and largely structured in Cretaceous time (Zanchetta et al., 2015). These units form a tectonic lid on top of the Cenozoic metamorphic units derived from the European paleomargin, which include the Lepontine dome in the Central Alps, and the accretionary wedge of the Western Alps (Fig. 1). On the southern side of the drainage, the Alpine wedge is partly masked by the wedge-top successions of the Tertiary Piedmont Basin, and includes the Ligurian units of the Northern Apennines that are stratigraphically overlain by Epiligurian sedimentary successions (Fig. 1). The underlying Subligurian and Tuscan units were accreted within the framework of Apenninic subduction, and include Oligo-Miocene turbidites fed from the exhuming Lepontine dome, originally deposited in the Adriatic foredeep (Garzanti and Malusà, 2008).

The Northern Apennines underwent subsidence during most of the Cenozoic. The Ligurian units were long buried by detritus eroded from the Alps, to be eventually uplifted and exhumed in Plio-Quaternary times (Malusà and Balestrieri, 2012). Large amounts of Alpine detritus were thus recycled and transferred to the Po Plain, which represents at the same time the Apenninic foredeep and the retrobelt basin of the Alps. The Plio-Quaternary sedimentary succession preserved in this basin is up to 8 km thick, and is deformed by S-dipping Apenninic thrusts still active today (Ghielmi et al., 2013). Subsidence rates in the Po Plain have remained high throughout the Quaternary (> 1mm/yr; Carminati and Di Donato, 1999), even when the Pliocene to Early Pleistocene marine sedimentation was replaced by continental sedimentation (Ghielmi et al., 2013). After the onset of major Pleistocene glaciations, large moraine amphitheaters formed on the southern side of the Alps, and some of them now dam deeply eroded postglacial lakes (425 m water depth in Lake Como, Fig. 1). Today, the Po basin is one of the most intensively cultivated and populated areas in Europe, hosting >20 million people. The source-to-sink connectivity in the basin is thus disturbed by both natural processes and heavy human modifications, including >100 large dams and reservoirs (Fig. 2).

## 3. SAMPLING STRATEGY

We collected bedload river sand samples of 25 tributaries (T1-T24, plus sample O1 collected outside the Po catchment), 9 samples from the Po Plain (P1-P9), and 3 samples from the Po delta (D1-D3) (Fig. 1 and Supplement Table S1). This sample suite includes samples from both upstream and downstream of Lake Maggiore, and compares, on the scale of the entire Po basin, basins not affected by dams (T5, T6, T9, T10, T16, T17, T19, T22, samples "Verz" by Wittmann et al. (2007) and the entire dataset by Norton et al. (2011)) to those where sediment output is potentially modified by the presence of dams (i.e. all other basins). Post-glacial lakes and dams provide longer-term and short-term sinks of sediment that disturb the basin´s connectivity. We also tested the influence of large moraine amphitheaters (P4-P5 for the Ticino and T12-T13 for the Dora Baltea amphitheater, respectively) on the cosmogenic nuclide budget. Sediment may be trapped behind these features for significant periods, or may contribute non-steady state erosion products through undercutting to the river´s nuclide budget.

The cosmogenic-nuclide concentrations acquired during erosion in the source may either decrease in the floodplain, because of radionuclide decay during sediment burial, or increase by additional nuclide production during surficial lowland sediment transport. Although the production rate in buried sediments is reduced due to shielding from cosmic irradiation, the potential decrease in nuclide concentration in reworked sediment is generally limited by the long half-life of $^{10}$Be (~1.4 Myr), which is notably longer than the storage time in most floodplains (Wittmann and von Blanckenburg, 2009). Sediment burial in lowland settings can be proficiently assessed using the *in situ* $^{26}$Al/$^{10}$Be ratio (Wittmann et al., 2011b), which in the lack of deep sediment storage should be ~6.5-7.0 (i.e. close to the ratio of the individual surface production rates of these nuclides; Granger, 2006). In case of sufficiently deep storage before reworking, instead, the $^{26}$Al/$^{10}$Be ratio decreases because of faster radioactive decay of $^{26}$Al (half life of ~0.7 Myr) compared to $^{10}$Be (Wittmann et al., 2011b). To monitor sediment storage and reworking in the floodplain, we measured the concentrations of *in situ* $^{26}$Al in 13 samples, distributed among the different source areas and the Po Plain. For tributary sample T3, Po Plain samples P1, P3 and P6, and Po delta samples D1 and D2, we also analyzed noble gases to determine the concentration of cosmogenic $^{21}$Ne and monitor any potential increase in cosmogenic nuclide concentration by additional production during surficial sediment transport. Such a potential increase should be proportional to a minimum time of near-surface bedload transport (e.g., in

exposed sand bars), but is expected to be low because of the low overall nuclide production rate in low-elevation floodplains.

We complemented our dataset with $^{10}$Be data for the Central Alps previously published by Wittmann et al. (2007) and Norton et al. (2011) (Fig. 1 and Tables S2, S3). We also considered literature $^{10}$Be data from the Adige catchment in the Eastern Alps (Norton et al., 2011), now outside the Po drainage, because the Adige River and the Pleistocene Adige-Garda glacier may have provided sediment to the Po Plain before the post-LGM (Last Glacial Maximum) drainage re-organization (see Fig. 1). Because of the long half-life of $^{10}$Be, a cosmogenic signal originally derived from the Eastern Alps may be still present in the sediments of the Po Plain.

## 4. METHODS

### 4.1. Determination of *in situ* cosmogenic Be and Al

Samples were sieved (analyzed size fractions are reported in Supplement Table S1) and processed using the revised method of von Blanckenburg et al. (2004) to separate *in situ*-produced $^{10}$Be from the sample matrix. We added 0.4 g of a $^{9}$Be carrier with a concentration of 372 ppm to each sample, whose $^{10}$Be amount was determined from measurements of one process blank per sample batch. The resulting $^{10}$Be contained in each blank that was included in the blank correction is given in Table 1A,B. Simultaneous separation of cosmogenic $^{26}$Al and stable $^{27}$Al involved additional steps. Al blanks (but not the samples) were spiked with 0.4 g of a Merck© Al ICP standard with a concentration of 1000 ppm to monitor Al background levels. For this Al blank carrier, we determined an average $^{26}$Al/$^{27}$Al ratio of $(6.5\pm5.4)\times10^{-15}$ (±1SD, n = 3). After Fe, Be and Al column chemistry, respectively, and alkaline precipitation, samples were calcinated and pressed into accelerator mass spectrometer (AMS) cathodes. Both cosmogenic $^{10}$Be and $^{26}$Al were measured at the Cologne University AMS facility (Dewald et al., 2013). Stable Al concentrations of samples were determined from splits of digested sample solutions using optical emission spectroscopy (OES, Varian) and their concentrations were validated against matrix effects and interferences by carrying out external monitoring using reference materials. For detailed description of separation procedures, reference materials used, and AMS standardization, we refer to the supplementary information (Text S1).

### 4.2. Determination of *in situ* cosmogenic Ne

Quartz samples to be analyzed for cosmogenic $^{21}$Ne were ground to <100 µm in an agate mill, in order to reduce the contribution of atmosphere-like Ne trapped in fluid inclusions. To check the isotopic composition of Ne trapped in fluid inclusions, aliquots of three samples (T3, D1, D2) were crushed in vacuo and the noble gases analyzed. For heating extractions, all samples were wrapped in Al foil and loaded to the sample carrousel above the extraction furnace, which was baked beforehand at 100°C for about one week. Noble gases were extracted by stepwise heating (at 400°, 600°, 800°, and 1200° C, see Table S3) for 20 minutes each. After gas extraction, by either heating or crushing, chemically active gases were removed in two Ti sponge getters and two SAES (ZrAl) getters, Ar-Kr-Xe were trapped in a charcoal finger at liquid nitrogen temperature, and He and Ne separated from each other by trapping in a cryogenic adsorber at 11 K and subsequent sequential release. He and Ne concentrations and isotopic compositions were determined in a MM5400 sector field mass spectrometer, and were corrected for isobaric interferences, instrumental mass fractionation and analytical blanks (Niedermann et al., 1997). An aliquot of the quartz standard CREU-1 was measured during the same batch of samples and yielded a $^{21}$Ne excess of (348±13) $\times 10^6$ at/g, in excellent agreement with the reference concentration of (348±10)$\times 10^6$ at/g (Vermeesch et al., 2015).

### 4.3. Calculation of $^{10}$Be production rates

Calculation of the basin-wide total $^{10}$Be production rate $\bar{P}$ (at/$g_{QTZ}$/yr) was carried out for each pixel in a 90 m digital elevation model (DEM). We used the time-independent scaling model of Dunai (2000), calibrated to a sea-level high latitude (SLHL) spallogenic $^{10}$Be production rate of 3.7 at/$g_{QTZ}$/yr (e.g. Phillips et al., 2016). The total SLHL production rate of 3.75 at/$g_{QTZ}$/yr used includes the muon parametrization of Braucher et al. (2011), indicating a ca. 1% muon contribution at SLHL. When calculating the source-area production rate $P_{source}$ (in at/$g_{QTZ}$/yr) over the basin´s source area, $A_{source}$, which excludes a lowland contribution, we used a sliding window for elevation variance. If the standard deviation fell below a value of 25 m within an area of 15x15 pixels (90 m DEM, corresponding to an area of 1.8 km$^2$), the central pixel was considered as low-relief

floodplain. This approach has proven robust against pixel-dependent variations in topography and elevation outliers.

To identify areas dominated by quartz-free carbonate rocks, mainly present in the eastern Central Alps, we used the maps of the Italian Geological Survey (http://www.isprambiente.gov.it/it/cartografia). These quartz-free areas were not included in production rate calculation. We did however not specifically exclude topographic areas located upstream of dams or lakes.

Topographic shielding was accounted for following Wittmann et al. (2007), and shielding due to modern ice cover was accounted for by clipping ice-covered area from the DEM derived from the global lithological map database "GLIM" (Hartmann and Moosdorf, 2012). Correction factors of the production rate for shielding due to snow cover are based on mean averages of snow thickness maps for the years 1921 – 1960 derived from the Ministero dei Lavori Pubblici (1960). Following the approach by Wittmann et al. (2007), the average snow thickness, a snow density of 0.3 g/cm$^3$, and a cosmic ray attenuation length of 157 g/cm$^2$ were used in Equation 5 of Wittmann et al. (2007), to derive a correction factor that was then multiplied by the nucleonic surface production rate, leaving all other (i.e. muonic) coefficients of Braucher et al. (2011) constant (see below). This approach is justified by the weak interaction of muons with low-density materials such as snow.

Processing of published data included in this study (Wittmann et al., 2007; Norton et al., 2011) encompassed the recalculation of published $^{10}$Be production rates according to the above scaling model and SLHL production rates. To allow for direct comparison of published $^{10}$Be concentrations with data measured relative to new AMS standards (as a result of the 2010 newly determined $^{10}$Be half-life of 1.387 Myr; e.g. Chmeleff et al., 2010), we reduced published $^{10}$Be data, based on the old standardization with a 1.51 Myr half life, by a factor of 1.096 (e.g. Kubik and Christl, 2010).

### 4.4. Calculation of denudation rates and sediment fluxes

Sediment leaving the source area of a river basin attains a steady state *in situ* cosmogenic $^{10}$Be concentration (termed [$^{10}$Be], at/g$_{QTZ}$) if the export by erosion is equal to the rate of $^{10}$Be production, and if

denudation has been steady over sufficiently long time scales (von Blanckenburg, 2005). We calculated basin-wide denudation rates $D_{insitu}$ (cm/yr) using *Equation 1* (Brown et al., 1995):

$$D_{insitu} = \frac{1}{[^{10}Be]\times\rho} \times \left(\bar{P}_{n_i} \times \Lambda_{n_i} + \bar{P}_{\mu s_i} \times \Lambda_{\mu s_i} + \bar{P}_{\mu f_i} \times \Lambda_{\mu f_i}\right) \quad \textit{Equation 1}$$

where $\bar{P}_{n_i}, \bar{P}_{\mu s_i}, \bar{P}_{\mu f_i}$ are the pixel-averaged basin-wide $^{10}$Be production rates (at/$g_{QTZ}$/yr) for neutrons, slow muons, and fast muons, respectively, with $\Lambda_{n_i}, \Lambda_{\mu s_i}, \Lambda_{\mu f_i}$ being the effective attenuation lengths of neutrons (157 g/cm$^2$), slow muons (1500 g/cm$^2$), and fast muons (4320 g/cm$^2$), respectively (Braucher et al., 2011). The density of removed rock or soil is given by $\rho$ (g/cm$^3$). The term $\rho/\Lambda_n$ is often replaced by z*, the absorption depth scale (cm), which is the distance over which the cosmic-ray flux decreases by a factor of *e*, or 63%. This vertical distance, divided by the denudation rate, gives the erosional integration time scale of the method (von Blanckenburg, 2005). We neglected decay of $^{10}$Be (decay constant of $^{10}$Be is $5\times10^{-7}$ yr$^{-1}$) in equation 1, because even in settings eroding as slow as ca. 0.3 mm/kyr, time scales of decay are much longer than erosional integration time scale (von Blanckenburg, 2005).

On the scale of an entire foreland basin or regions such as the Alps or Apennines, it is necessary to evaluate a mean "signal" (i.e. nuclide concentration, denudation rate, or sediment flux) that is representative for the region. In order to derive such a representative signal from a set of samples from tributaries, we prefer to calculate "area-weighted" values, in order not to over-represent small, nested catchments by simply calculating mean values. The following equation accounts for this "area-weighting" for the example of an area-weighted denudation rate $\overline{D_{insitu}}$ (mm/yr):

$$\overline{D_{insitu}} = \frac{\sum_{i=1}^{n}(A_{(source)_n} \times D_{(insitu)_n})}{\sum_{i=1}^{n} A_{(source)_n}} \quad \textit{Equation 2}$$

Equation 1 is only valid if denudation has been steady over the time it takes to erode several absorption depth scales. Sediment interception and storage by dams or lakes may violate the steady-state assumption, because sediment may accumulate additional cosmogenic nuclides while being stored, or cosmogenic

nuclide concentrations may decrease due to decay when deeply buried (Granger et al., 1996). If no deep sediment storage occurs, then $^{10}$Be concentrations carried by sediment through a basin preserve their value of the source areas or slightly increase (Wittmann and von Blanckenburg, 2009). Importantly, however, $^{10}$Be concentrations do not decrease because the $^{10}$Be half-life is long compared to sediment storage times in most floodplains (Wittmann and von Blanckenburg, 2009). Indeed, we show in section 6.1 that the sediment in the Po Plain is mainly produced in the source area and has inherited the respective nuclide concentration fingerprint. For such a case, the so-called floodplain correction (Wittmann et al., 2009) is carried out, which couples the source-area $^{10}$Be production rate $P_{source}$ calculated for the high-elevation source area to the $^{10}$Be concentration measured in lowland sediment, termed $[^{10}Be]_{lowl}$ (at/$g_{QTZ}$) that is thought to be representative of the entire source area erosion process. By doing so, the lowland component of the total, basin-wide production rate $\bar{P}$ is ignored (Wittmann et al., 2009; 2011a), such that in *Equation 3*, only $P_{source}$ is used to derive a floodplain corrected denudation rate $D_{insituFC}$:

$$D_{insituFC} = \frac{1}{[^{10}Be]_{lowl} \times \rho} \times \left(P_{n-source_i} \times \Lambda_{n_i} + P_{\mu s-source_i} \times \Lambda_{\mu s_i} + P_{\mu f-source_i} \times \Lambda_{\mu f_i}\right) \qquad \textit{Equation 3}$$

Floodplain-corrected denudation rates, in m/yr, can be converted into floodplain-corrected sediment fluxes $QS_{insituFC}$ (kg/yr) assuming an average rock density (ρ=2,700 kg/m$^3$) and using the basin area (m$^2$) upstream of the sampling point:

$$\mathrm{QS_{insituFC}} = \mathrm{D_{insituFC}} \times \mathrm{A_{source}} \times \rho \qquad \textit{Equation 4}$$

where $A_{source}$ is the high-relief source area of the basin (see Supplement Table S1) calculated using the elevation variance method described above.

## 5. RESULTS

### 5.1. *In situ* cosmogenic $^{10}$Be concentrations

The *in situ* $^{10}$Be concentrations in the analyzed samples (Table 1A,B, Fig. 3A) range from 0.83×10$^4$ at/$g_{QTZ}$ (sample T8, Toce at Ornavasso) to 6.52×10$^4$ at/$g_{QTZ}$ (sample T10, Craso del Gallo). Area-weighted $[^{10}Be]$ values

276 ($[\overline{^{10}Be}]$) and, if not otherwise stated, area-weighted 1σ uncertainties for each sample group were calculated
277 according to equation 2 as smaller tributaries contribute less sediment and are spatially less representative
278 (Fig. 3). These $[\overline{^{10}Be}]$ values range from (1.18±0.30)×$10^4$ at/$g_{QTZ}$ in the Northern Apennines (n = 5, samples
279 T20-T24) to (5.85±0.26)×$10^4$ at/$g_{QTZ}$ in the southern Western Alps (n = 2, samples T16-T17). In the eastern
280 Central Alps, $[\overline{^{10}Be}]$ values of (1.71±0.14)×$10^4$ at/$g_{QTZ}$ (n=11, including samples T1, T2 and 9 samples from
281 Norton et al., 2011) are found that are similar to those in the western Central Alps ((2.04±0.24)×$10^4$ at/$g_{QTZ}$;
282 n=17, including samples T5-T11 and 10 samples from Wittmann et al., 2007), and the northern Western Alps
283 ((1.98±0.13)×$10^4$ at/$g_{QTZ}$; n = 4, samples T12-T15). Somewhat higher $[\overline{^{10}Be}]$ values on the order of ~3×$10^4$
284 at/$g_{QTZ}$ are found in river sands derived from the Ligurian Alps and the overlying Tertiary Piedmont basin
285 ((3.17±0.14)×$10^4$ at/$g_{QTZ}$; samples T18, T19 and P2), and in the Adige catchment ((3.41±0.45)×$10^4$ at/$g_{QTZ}$; 12
286 samples from Norton et al., 2011).
287
288
289 **5.2. *In situ* $^{10}$Be-derived denudation rates**
290 *In situ* $^{10}$Be-derived denudation rates (Figures 2 and 3B) range from 0.08 mm/yr (sample T10) to 1.48
291 mm/yr (sample T8) in mountain catchments (Table 1A). Floodplain-corrected denudation rates recorded by
292 lowland samples range from 0.17 mm/yr (sample P2) to 0.51 mm/yr (sample P5). The highest denudation
293 rates are found in the Toce basin of the western Central Alps (1.48 mm/yr), where they are on the order of
294 those measured by Wittmann et al. (2007) at different locations within the same catchments. Wittmann et
295 al. (2007) observed differences in denudation rates with grain size by a factor of ~2 that however showed no
296 clear association of e.g. the coarser fraction having higher denudation rates, as it would be the case if
297 landslide material would be preferentially incorporated. We have not analyzed different samples for different
298 grain size fractions, and such variability may be contained in our data as well. Although denudation rates of
299 roughly 0.5 to 1 mm/yr are found in most of the northern Western Alps (0.81 mm/yr for T15) and eastern
300 and western Central Alps (0.70-0.85 mm/yr; samples T1, T3-T4), also much lower denudation rates are
301 observed in close vicinity (for example for samples T5-T6 and T9-T11, 0.08-0.29 mm/yr). These more slowly

eroding catchments were, according to the available maps (e.g. Ehlers and Gibbard, 2004), also glaciated during the LGM and have similar rock erodibilities (Kuehni and Pfiffner, 2001), but notably lower mean elevations (Supplement Table S1). A $\overline{D_{insitu}}$ of the Po-draining Alpine basins denotes to 0.49±0.33 mm/yr (n=37; uncertainty given here is 1SD of the dataset to highlight its variability). The low denudation rates recorded in the Tertiary Piedmont basin (0.15 mm/yr; sample T19) markedly increase in the Northern Apennines (0.38-0.47 mm/yr; samples T21-T24). Apenninic catchments may show denudation rates comparable with several Alpine catchments, despite their gentle topography (relief <2000 m and slope values of 13°-17° - Supplement Table S1) as a result of the higher erodibility of Apenninic sedimentary rocks. These results are in line with the denudation rates reported by Cyr and Granger (2008), who studied Apenninic catchments ~200 km south of our sampling sites, and with exhumation rates provided by fission-track analysis on detrital apatite (Malusà and Balestrieri, 2012). A $\overline{D_{insitu}}$ of the Apennine basins denotes to 0.44±0.11 mm/yr (again, uncertainty given here is 1SD of the dataset).

### 5.3. *In situ* $^{10}$Be-derived sediment fluxes

In Alpine mountain catchments, *in situ* $^{10}$Be-derived sediment fluxes range from >5 Mt/yr in the Dora Baltea upstream of the Ivrea moraine amphitheater (sample T12), the Toce at Orvanasso (sample T8) and the Adda at Dubino (sample T1) to <0.1 Mt/yr in the small catchments of the western Central Alps (samples T5-T6 and T9-T10) and in the upper Po (sample T16) (Fig. 2). Summing up all Alpine tributaries (i.e. ignoring smaller nested catchments) measured upstream of lake influence, the total cosmogenic $^{10}$Be-derived sediment flux ($QS_{insitu}$) is 27 Mt/yr. This mass flux accounts for ~93% (~23,500 km$^2$) of the Alps draining into the Po basin (i.e., areas dominated by carbonate rocks in Southalpine and Austroalpine domains are excluded from this calculation). A total $QS_{insitu}$ cosmogenic $^{10}$Be-derived sediment flux for the Apennines, encompassing a much smaller area of the Po basin than the Alps, amounts to 5.1 Mt/yr.

### 5.4. *In situ* cosmogenic $^{26}$Al concentrations and $^{10}$Be/$^{26}$Al ratios

The *in situ* $^{26}Al$ concentrations and $^{26}Al/^{10}Be$ ratios derived from our analyses are reported in Table 2. The $^{26}Al$ concentrations in mountain catchments range from ~$9\times10^4$ at/$g_{QTZ}$ (samples T15 and T24) to ~$35\times10^4$ at/$g_{QTZ}$ (samples T16 and T17). An area-weighted $^{26}Al$ concentration ($[\overline{^{26}Al}]$) for the source areas is $(16.6\pm2.5)\times10^4$ at/$g_{QTZ}$. For the two Apenninic samples (T23 and T24), the analytical uncertainties are very high (~20% on the $^{26}Al/^{27}Al$ AMS ratio, Table 2), due to very low (in the lower $10^{-14}$) $^{26}Al/^{27}Al$ ratios and concurrent high $^{27}Al$ concentrations. For the Po Plain, the $[\overline{^{26}Al}]$ is $(17.6\pm3.1)\times10^4$ at/$g_{QTZ}$.

The resulting $^{26}Al/^{10}Be$ ratios, also reported in Table 2, are in accordance with the surface production rate ratio of these nuclides (~6.5 to 7; e.g. Goethals et al., 2009), and thus do not show a sediment-burial signal. The much higher $^{26}Al/^{10}Be$ ratios in the Apennine samples are most likely analytical artifacts.

### 5.5. *In situ* cosmogenic $^{21}Ne$ concentrations

The $^{21}Ne/^{20}Ne$ ratios in the analyzed samples are only marginally higher than the atmospheric value of 0.002959 (Eberhardt et al., 1965), thus reflecting only minor (cosmogenic) $^{21}Ne$ excesses. The decomposition of different Ne components to calculate $^{21}Ne$ excesses for such close-to-air ranges is not trivial, because of the possible presence of non-atmospheric trapped and nucleogenic Ne (Fig. 4). Trapped Ne can comprise atmospheric, mantle, or crustal gases (possibly slightly fractionated) residing mainly in fluid inclusions (Niedermann, 2002). Nucleogenic Ne is produced *in situ* through the $^{18}O(\alpha,n)^{21}Ne$ reaction and the $^{19}F(\alpha,n)^{22}Na(\beta^+)^{22}Ne$ reaction, respectively, when high concentrations of U and Th in granitic rocks deliver non-negligible amounts of $\alpha$ particles, a process most important in old rocks (Niedermann, 2002). Depending on the O/F ratio in minerals where production takes place, in a three-isotope diagram of $^{22}Ne/^{20}Ne$ versus $^{21}Ne/^{20}Ne$, nucleogenic Ne may plot above or below the "spallation line", i.e. the mixing line between atmospheric Ne ($^{21}Ne/^{20}Ne$ = 0.002959 and $^{22}Ne/^{20}Ne$ = 0.1020; Eberhardt et al., 1965) and cosmogenic Ne (Niedermann et al., 1993).

The Ne three-isotope plot (Fig. 4) shows that most 400-800°C data plot above the spallation line, at $^{21}Ne/^{20}Ne$ ratios <0.004. In contrast, the 1200°C steps (not shown in Fig. 4 because out of scale) plot below the line at considerably higher $^{21}Ne/^{20}Ne$ up to 0.019 (not blank-corrected), although uncertainties are large

due to low Ne amounts within the blank range in that step. The 1200°C pattern is quite typical for old rocks (e.g. Kounov et al., 2015) and indicates the presence of a nucleogenic $^{21}Ne$ component that is degassed at temperatures >800°C. The ≤800°C steps, however, where the release of cosmogenic Ne is expected (Niedermann, 2002), exhibit an unusual pattern. Most data are arranged along a steep trend, with only a few (all belonging to samples D1 and D2) plotting to the right of that trend. The steep trend, which also includes the crusher data, i.e. the presumed composition of trapped Ne, is consistent with a nucleogenic Ne signature having a fixed $^{21}Ne/^{22}Ne$ production ratio. If so, then the samples from the upper Po basin contain only negligible amounts of cosmogenic Ne, but a characteristic nucleogenic Ne component produced in the predominant lithologies. The Po delta samples are likely to carry the same nucleogenic Ne component, but judging from the position of their data in Fig. 4 they seem to contain some additional cosmogenic Ne.

Because regular procedures of $^{21}Ne$ excess calculations (Niedermann, 2002) cannot be followed to investigate these observations, we present new means to estimate approximate cosmogenic $^{21}Ne$ concentrations in Po delta samples, as explained in detail in the supplementary section (Text S2). Using that method, we calculate $^{21}Ne$ excesses of 1.56 (+0.75/-0.68)×$10^6$ at/$g_{QTZ}$ for sample D1 and 0.7 (+1.5/-0.6)×$10^6$ at/$g_{QTZ}$ for sample D2. Note that the 2σ uncertainties given include only analytical uncertainties of the step-heating data, but not the notably high uncertainty of the non-cosmogenic component, which depends to a large extent on the uncertainty of the nucleogenic correlation line (Fig. 4), and thus on the validity of the assumptions. Clearly, under these circumstances, the results can only provide a rough estimate of the real cosmogenic $^{21}Ne$ content of the delta samples.

## 6. DISCUSSION

In this section, we use our dataset to: (i) investigate the propagation of the cosmogenic signal from the source areas to the delta; (ii) assess the impact of deep lakes, moraines and large dams on the $^{10}Be$ signal; and (iii) compare the cosmogenic nuclide-derived sediment fluxes with the estimates based on gauging and discuss the potential causes of discrepancy between the two methods.

### 6.1. Propagation of the cosmogenic signals from the source areas to the delta

Figure 3 shows the *in situ* $^{10}$Be concentrations and the $^{10}$Be-derived denudation rates plotted versus the distance of the analyzed samples from the Po delta. The high variability in [$^{10}$Be] and $^{10}$Be-derived denudation rates in the source areas progressively decreases with increasing lowland area. A more detailed evaluation of $^{10}$Be patterns shows that the $[\overline{^{10}Be}]$ value (±1σ area-weighted uncertainties) of the lowland samples upstream of the Po-Ticino confluence ((3.61±0.19)×10$^4$ at/$g_{QTZ}$; samples P1, P3-1, P3-2) is notably higher than the $[\overline{^{10}Be}]$ value (using $A_{total}$ in equation 2) of all the lowland samples ((2.62±0.17)×10$^4$ at/$g_{QTZ}$; n = 13; samples P1, P3-P9, D1-D3). The value of 3.61×10$^4$ at/$g_{QTZ}$ mainly reflects the [$^{10}$Be] values measured in the catchments of the southern Western Alps. The pronounced decrease in [$^{10}$Be] observed downstream of the Ticino-Po confluence (~3.08×10$^4$ at/$g_{QTZ}$ at site P6, Po at Zerbo) is ascribed to the low [$^{10}$Be] of the Ticino bedload (1.31×10$^4$ at/$g_{QTZ}$; samples P4-P5), which is inherited from the rapidly eroding source areas of the western Central Alps (Fig. 2, Table 1A). Downstream of sample P6, the [$^{10}$Be] progressively decreases towards a value similar to the $[\overline{^{10}Be}]$ value of all lowland samples, reaching 2.1-2.6×10$^4$ at/$g_{QTZ}$ at the delta. This decrease is partly due to the addition of sediment from the rapidly eroding Apennines, having very low [$^{10}$Be], but could also reflect somewhat delayed mixing of sediment from the Ticino branch with sediment from the Po branch (see Section 6.2). The slight increase in [$^{10}$Be] measured between samples P8 and P9 (2.13×10$^4$ vs. 2.41×10$^4$ at/$g_{QTZ}$), and a somewhat higher [$^{10}$Be] observed in the northernmost delta sample (D1) compared to samples D2 and D3 (see Table 1B), might reflect mixing of Po sediments with higher [$^{10}$Be] lowland sediment derived from the upper Adige in pre-glacial times ($[\overline{^{10}Be}]$ = (3.01±0.41)×10$^4$ at/$g_{QTZ}$, n = 12).

The broad trend that we observe for [$^{10}$Be] across the Po floodplain (red dots in Fig. 3) is thus dominated by the preservation of a mean source area-derived $^{10}$Be signal from both the Alps and the Apennines, reduced in variability in the lower part of the catchment. This behavior has been observed in the Amazon Beni basin and in the Ganga basin (Wittmann et al., 2009; Lupker et al., 2012).

Our $^{26}$Al dataset confirms these observations. The [$^{26}$Al] shows a sharp decrease downstream of the Ticino-Po confluence, from ~23.6×10$^4$ at/$g_{QTZ}$ (site P3) to ~17.4×10$^4$ at/$g_{QTZ}$ (site P6), which is consistent with

406 mixing of Po sediment derived from the northern Western Alps with sediment having lower cosmogenic
407 nuclide concentrations derived from the western Central Alps. The $^{26}$Al dataset also confirms the higher
408 cosmogenic nuclide concentration observed in the northernmost delta sample (~$23.6\times10^4$ at/$g_{QTZ}$ in sample
409 D1) compared to the other delta samples, which may reflect the mixing of Po sediments with sediment
410 originally derived from the Adige catchment. Moreover, the measured $^{26}$Al/$^{10}$Be ratios in our samples exclude
411 any major modification of the source-derived $^{10}$Be signal due to the addition of deeply buried floodplain
412 material. This is in line with the fast subsidence characterizing the Po Plain, and with the presence of stable,
413 superelevated levees that limit the sediment exchange between the channel and the floodplain in the lower
414 part of the basin. In this situation, the sediment carried in the channel is dominated by the cosmogenic signal
415 derived from the source area.

416 In such favorable conditions, the accumulation of cosmogenic nuclides during transport across the
417 lowlands may be resolvable, thus allowing calculation of the sediment residence time in the floodplain, if the
418 depth-integrated production rate during transfer of sediment through the floodplain is known and if decay
419 of nuclides during residence is negligible (i.e. indeed recorded in the Po plain by $^{26}$Al/$^{10}$Be ratios of 6.5-7). By
420 measuring $^{21}$Ne across the Po Plain, we aimed for an independent estimation of sediment residence time,
421 because $^{21}$Ne is a stable (non-decaying) cosmogenic noble gas that is, in theory, more sensitive to exposure
422 than $^{10}$Be due to its higher production rate. However, $^{10}$Be should also record an increase in sediment
423 residence because its relative detection limit is much lower than that of $^{21}$Ne. In the Po plain, our near-
424 detection-limit analyses cannot unambiguously detect sediment residence; a corresponding estimate would
425 be as high as 45 kyr using the lower 2σ error bound of sample D1 of $0.88\times10^6$ at/$g_{QTZ}$ in $^{21}$Ne excess and a
426 total $^{21}$Ne production rate of 16.7 at/$g_{QTZ}$/yr (Goethals et al., 2009). Given these boundary conditions, we
427 regard it as more likely that the $^{21}$Ne excess values result from a previous exposure episode during the Alpine
428 orogeny, as Apenninic units include recycled Alpine material (Garzanti and Malusà, 2008; Malusà and
429 Balestrieri, 2012).

430

431 **6.2. Impact of lakes, moraines and dams on the $^{10}$Be signal**

The deep lakes of the Southern Alps are superimposed on an Oligo-Miocene drainage network overincised during the Messinian salinity crisis (Garzanti and Malusà, 2008), and acquired their present form during ice retreat in late LGM times, ~17 kyr ago (Hinderer, 2001). These lakes now separate the upper reaches of major Po tributaries (e.g., Ticino, Adda) from their lower reaches, and store sediment derived from the Alps over timescales that are relevant for cosmogenic nuclide-based denudation. We assess the bias on the cosmogenic-nuclide budget from sediment trapping based on two examples: (a) sediment-mixing calculations performed in areas downstream of lakes, and (b) close examination of sediment-flux data directly up- and downstream of lakes (see below).

(a) If we mix the cosmogenic nuclide concentrations of the lower Ticino at site P5 and the Po at site P3 in proportion to their sediment fluxes (using Equation 5 in von Blanckenburg et al., 2004), then we would expect a [$^{10}$Be] of 2.5×10$^4$ at/g$_{QTZ}$ below the Po-Ticino confluence (close to P6). This value (based on the following input values, see Table 1B): (i) $QS_{insituFC}$ = 10 Mt/yr at P5; (ii) $QS_{insituFC}$ = 12 Mt/yr at P3; and (iii) the mean [$^{10}$Be] for each river at sites P5 and P3, respectively) is lower than the actually measured [$^{10}$Be] value at sampling point P6 (mean of (3.1±0.2)×10$^4$ at/g$_{QTZ}$). Therefore, the ca. 20% higher [$^{10}$Be] value measured at sampling point P6 is either due local hydraulic effects in the river, leading to incomplete sediment mixing at the confluence, or it shows that the Ticino does not contribute sediment proportionally. In the latter case sediment fluxes below the confluence would be dominated by the Po branch, most likely because of sediment trapping in Lake Maggiore. If so, however, Figure 3 shows that this bias is negligible on the scale of the whole Po basin, meaning that with increasing distance downstream of a confluence, increased degrees of sediment mixing can be expected. In our case, [$^{10}$Be] of roughly 2.5×10$^4$ at/g$_{QTZ}$ are detected downstream of P8 (Po at Viadana) and P9 (Po at Castelnuovo).

Regarding (b), upstream and downstream of the lake, our $^{10}$Be dataset (Fig. 5) shows that the sum of the $^{10}$Be-derived sediment fluxes measured in major tributaries of Lake Maggiore (10.2±1.4 Mt/yr) is indistinguishable, within error, from the $^{10}$Be-derived sediment flux derived from sample P4, collected just downstream of the lake (8.7±0.6 Mt/yr). This suggests that: (i) sampling most likely was representative; (ii) denudation rates prior to lake formation were similar to today; and that (iii) even if sediment would leave the lake, its nuclide concentration would be unchanged because the $^{10}$Be accumulation during storage in the

lake can be considered negligible as the thick water mass attenuates the nuclide production at the lake bottom. The expected effect of $^{10}$Be radioactive decay during post-LGM storage is also negligible, because of the short timescale compared to the $^{10}$Be half-life.

The effect of large moraine amphitheaters on measured [$^{10}$Be] also appears negligible. The [$^{10}$Be] measured upstream of the large Dora Baltea amphitheater is indistinguishable within analytical error from the [$^{10}$Be] measured shortly downstream ((1.99±0.14)×10$^4$ at/g$_{QTZ}$ vs. (1.95±0.10)×10$^4$ at/g$_{QTZ}$), even in the lack of a deep lake (Fig. 5B). This suggests that the moraine material has reached steady state with regard to cosmogenic nuclides, and thus may erode at the same rate as the landscape upstream (cf., Wittmann et al., 2007). This is not surprising, because glacial till is widespread in the Dora Baltea catchment, and its preferential erosion, due to higher erodibility with respect to bedrock, may pose a bias on catchment-wide denudation rates. An alternative explanation of the unchanged [$^{10}$Be] below moraines is that the flux of river sediment originating from the upstream source is much higher than the local erosional flux of the moraine.

The role of dams and reservoirs in adjusting channel morphologies and retaining sediment is well-known (e.g. Vörösmarty et al., 2003). Hinderer et al. (2013) note that "half of the sediments mobilized in the headwaters do not reach the large valley rivers", although smaller runoff reservoirs ("cascades") are frequently flushed of their sediment and thus have little net trap efficiency. The timescale of sediment storage in reservoirs is short compared to the Alpine erosional timescale (apparent age of 1.5-2 kyr, Table 1A,B) as most Alpine reservoirs date from the 1950s and 1960s (Hinderer et al., 2013) and reservoirs are frequently evacuated to avoid siltation. Nevertheless, the existence of dams and reservoirs might have an impact on [$^{10}$Be] measurements (Hidy et al., 2014). Our data suggest that the large dams located upstream of Lake Maggiore (Fig. 5A) do not have a major impact on sediment fluxes. The impact of large dams and reservoirs appears negligible also on the scale of the whole Po basin (Fig. 3). The $[\overline{^{10}Be}]$ (± area-weighted 1 $\sigma$ uncertainties) of basins not influenced by dams ((2.93±0.32)×10$^4$ at/g$_{QTZ}$, n = 30) is close to the $[\overline{^{10}Be}]$ value ((2.29±0.19)×10$^4$ at/g$_{QTZ}$ (n=54)) obtained when all source area basins are included. Note that on the

485 small scale of a single watershed, however, the sediment sampled downstream of a dam may not adequately
486 represent the long-term denudation of the basin prior to dam construction. If this cannot be ruled out, we
487 suggest to exclude the upstream area from the calculation of cosmogenic nuclide production. We caution
488 however against doing so in every case, because sediment evacuation is a common process and the
489 integration timescale of the cosmogenic nuclide method should always be much longer than the life span of
490 the reservoirs.
491

492 **6.3. Cosmogenic nuclide-derived versus gauging-derived sediment fluxes**

493 The sediment fluxes derived from *in situ* $^{10}$Be measurements, $QS_{insitu}$ from source areas and $QS_{insituFC}$ in
494 the Po Plain, respectively, are compared, in Table 3, with the decadal timescale sediment fluxes ($QS_M$) mainly
495 derived from suspended-load measurements (Bartolini et al., 1996; Syvitski and Kettner, 2007; Hinderer et
496 al., 2013). The latter dataset covers ~50% of Alpine source areas, most Apenninic basins, and the Po Plain at
497 selected locations, allowing us to calculate a ratio of cosmogenic nuclide-derived to gauging-derived
498 sediment fluxes ($QS_{C/M}$ in Table 3). Because of sediment trapping in the subsiding Po Plain, $QS_{C/M}$ values are
499 expected to progressively increase from the source areas to the lowlands, reaching values >>1. We calculated
500 mean $QS_{C/M}$ ratios (±1SD) of 4.2 ± 2.4 for the Alps (n = 7) and of 3.3 ± 2.5 for the Apennines (n = 5). Similar
501 ratios of $QS_{C/M}$ of 4.6 ± 1.5 (n = 4) are obtained in the Po Plain. $QS_{C/M}$ ratios >>1 are thus observed not only in
502 the lowlands but also in the source areas, which confirms the observations of Wittmann et al. (2007) in the
503 Central Alps. These authors discussed the discrepancy to $^{10}$Be-derived denudation rates in detail, for example
504 suggesting that landslides in mountain basins may cause potential incorporation of $^{10}$Be-depleted landslide
505 material into the river network (e.g., Dora Riparia catchment; cf. Agliardi et al., 2013), thereby biasing $^{10}$Be-
506 derived denudation rates to higher values. However, gauging-derived sediment fluxes are well-known to
507 largely underestimate the total sediment flux. They do not generally include bedload, do not incorporate
508 large infrequent sediment transport events, and do not account for the large amount of sediment trapped in
509 subsiding lowlands (Fig. 6). Therefore, it is not surprising that global datasets comparing modern gauging-
510 derived and cosmogenic nuclide-derived loads in rapidly eroding settings (Covault et al., 2013) show that

nearly two-thirds of cosmogenic nuclide-derived loads exceed gauging-derived loads when measured at approximately the same location. Such an observation seems to be the rule, showing that our comparison agrees with global trends.

## 7. CONCLUSION

This study demonstrates that cosmogenic nuclides are a reliable tracer of mountain erosion and sediment transport even in foreland basins where the source-to-sink connectivity is disturbed by tectonic subsidence, sediment trapping in lakes and dams and intense human activity. We show that the cosmogenic record of Alpine and Apenninic erosion is effectively transmitted across the Po Plain from the source areas to the final depositional site in the delta. This cosmogenic record is virtually insensitive to a range of potential geological and anthropogenic sources of bias, and is largely independent from upstream sediment interception and floodplain sediment storage. For example, the similarity between $^{10}$Be nuclide concentrations measured upstream and downstream of the Lake Maggiore suggests that denudation rates prior to lake formation were similar to today. Reworking of deeply buried material in the floodplain, which may modify the source-derived $^{10}$Be signal, is limited by rapid tectonic subsidence. Tectonic subsidence therefore provides no obstacle for the application of long-lived cosmogenic nuclides to derive sediment fluxes, whereas it is problematic for present-day sediment fluxes derived from gauging. These results confirm the robustness of the cosmogenic-nuclide approach in source-to-sink studies and thus provide an integrated approach so that sediment routing from the sediment source to the floodplain sink can be quantified.

**Acknowledgements**

Work funded by DFG Project WI 3874/3-1 to H.W. and M.M. We thank C. Schulz, H. Haedke, N. Dannhaus, E. Schnabel and J. Bartel for lab support, and K. Norton for sharing basin delineations. We sincerely thank S. Heinze and S. Binnie from Cologne University for performing AMS measurements, as well as P.H. Blard and P. Vermeesch for constructive comments on this manuscript.

## References


1. Agliardi, F., Crosta, G.B., Frattini, P., Malusà, M.G., 2013. Giant non-catastrophic landslides and the long-term exhumation of the European Alps. Earth Planet. Sci. Lett. 365, 263-274.

2. Armitage, J.J., Dunkley Jones, T., Duller, R.A., Whittaker, A.C., Allen, P.A., 2013. Temporal buffering of climate-driven sediment flux cycles by transient catchment response. Earth Planet. Sci. Lett. 369-370, 200-210.

3. Autorità di Bacino del Fiume Po, 2001. Progetto di piano stralcio per l´assetto idrogeologico (PAI). Parma, Supplemento Straordinario della Gazzetta Ufficiale 166.

4. Bartolini, C., Caputo, R., Pieri, M., 1996. Pliocene—Quaternary sedimentation in the Northern Apennine Foredeep and related denudation. Geol. Mag. 133, 255-273.

5. Braucher, R., Merchel, S., Borgomano, J., and D. L. Bourlès, D.L., 2011. Production of cosmogenic radionuclides at great depth: A multi element approach, Earth Planet. Sci. Lett., 309(1-2), 1-9.

6. Brown, E.T., Stallard, R.F., Larsen, M.C., Raisbeck, G.M., Yiou, F., 1995. Denudation rates determined from the accumulation of in situ-produced $^{10}$Be in the Luquillo experimental forest, Puerto Rico. Earth Planet. Sci. Lett. 129, 193-202.

7. Carminati, E., Di Donato, G., 1999. Separating natural and anthropogenic vertical movements in fast subsiding areas: the Po plain (N. Italy) case. Geophys. Res. Lett. 26, 2291-2294.

8. Chmeleff, J., von Blanckenburg, F., Kossert, K., Jakob, D., 2010. Determination of the $^{10}$Be half-life by multicollector ICP-MS and liquid scintillation counting. Nuclear Instruments & Methods in Physics Research Section B- Beam Interactions with Materials and Atoms 268, 192-199.

9. Covault, J.A., Craddock, W.H., Romans, B.W., Fildani, A., Gosai, M., 2013. Spatial and Temporal Variations in Landscape Evolution: Historic and Longer-Term Sediment Flux through Global Catchments. The Journal of Geology 121, 35-56.

10. Cyr, A.J., Granger, D.E., 2008. Dynamic equilibrium among erosion, river incision, and coastal uplift in the northern and central Apennines, Italy. Geology 36, 103-106.

11. Dewald, A., Heinze, S., Jolie, J., Zilges, A., Dunai, T., Rethemeyer, J., Melles, M., Staubwasser, M., Kuczewski, B., Richter, J., Radtke, U., von Blanckenburg, F., Klein, M., 2013. CologneAMS, a dedicated center for accelerator mass spectrometry in Germany. Nuclear Instruments and Methods in Physics Research Section B: Beam Interactions with Materials and Atoms 294, 18-23.

12. Dunai, T.J., 2000. Scaling factors for production rates of in situ produced cosmogenic nuclides: a critical reevaluation. Earth Planet. Sci. Lett. 176, 157-169.

13. Eberhardt, P., Eugster, O., Marti, K., 1965. A Redetermination of the Isotopic Composition of Atmospheric Neon. Zeitschrift für Naturforschung 20a, 623-624.

14. Ehlers, J., Gibbard, P.L., 2004. Quaternary glaciations: extent and chronology. Developments in Quaternary Science 2, Part 1: Europe. Elsevier, Amsterdam.

15. Garzanti, E., Malusà, M.G., 2008. The Oligocene Alps: Domal unroofing and drainage development during early orogenic growth. Earth Planet. Sci. Lett. 268, 487-500.

16. Garzanti, E., Vezzoli, G., Andò, S., 2011. Paleogeographic and paleodrainage changes during Pleistocene glaciations (Po Plain, Northern Italy). Earth Science Reviews, 105, 25–48

17. Ghielmi, M., Minervini, M., Nini, C., Rogledi, S., Rossi, M., 2013. Late Miocene–Middle Pleistocene sequences in the Po Plain–Northern Adriatic Sea (Italy): The stratigraphic record of modification phases affecting a complex foreland basin. Mar. Petrol. Geol. 42, 50-81.

18. Goethals, M.M., Hetzel, R., Niedermann, S., Wittmann, H., Fenton, C.R., Kubik, P., Christl, M., von Blanckenburg, F., 2009. An improved experimental determination of cosmogenic $^{10}Be/^{21}Ne$ and $^{26}Al/^{21}Ne$ production ratios in quartz. Earth Planet. Sci. Lett. 284, 187-198.

19. Granger, D.E., 2006. A review of burial dating methods using $^{26}Al$ and $^{10}Be$. In: L.L. Siame, D.L. Bourlès, E.T. Brown (eds.), In Situ-Produced Cosmogenic Nuclides and Quantification of Geological Processes. Geol. Soc. Am. Spec. Paper 415, 1-16.

20. Granger, D.E., Kirchner, J.W., Finkel, R., 1996. Spatially averaged long-term erosion rates measured from in situ-produced cosmogenic nuclides in alluvial sediment. J. Geol. 104, 249-257.

21. Handy, M.R., Schmid, S.M., Bousquet, R., Kissling, E., Bernoulli, D., 2010. Reconciling plate-tectonic reconstructions of Alpine Tethys with the geological-geophysical record of spreading and subduction in the Alps. Earth-Sci. Rev. 102, 121-158.

22. Hartmann, J., Moosdorf, N., 2012. The new global lithological map database GLiM: A representation of rock properties at the Earth surface. Geochem. Geophys. Geosyst. 13, Q12004, doi: 10.1029/2012GC004370.

23. Hidy, A.J., Gosse, J.C., Blum, M.D., Gibling, M.R., 2014. Glacial-interglacial variation in denudation rates from interior Texas, USA, established with cosmogenic nuclides. Earth Planet. Sci. Lett. 390, 209-221.

24. Hinderer, M., 2001. Late Quaternary denudation of the Alps, valley and lake fillings and modern river loads. Geodin. Acta 14, 231-263.

25. Hinderer, M., Kastowski, M., Kamelger, A., Bartolini, C., Schlunegger, F., 2013. River loads and modern denudation of the Alps - A review. Earth-Sci. Rev. 118, 11-44.

26. Jerolmack, D.J., Paola, C., 2010. Shredding of environmental signals by sediment transport. Geophys. Res. Lett. 37, L19401, doi: 10.1029/2010GL044638.

27. Kirchner, J.W., Finkel, R.C., Riebe, C.S., Granger, D.E., Clayton, J.L., King, J.G., Megahan, W.F., 2001. Mountain erosion over 10 yr, 10 k.y., and 10 m.y. time scales. Geology 29, 591-594.

28. Kounov, A., Niedermann, S., De Wit, M.J., Codilean, A.T., Viola, G., Andreoli, M., Christl, M., 2015. Cosmogenic $^{21}$Ne and $^{10}$Be reveal a more than 2 Ma alluvial fan flanking the Cape Mountains, South Africa. South African J. Geol. 118, 129-144.

29. Kuehni, A., Pfiffner, O.A., 2001. The relief of the Swiss Alps and adjacent areas and its relation to lithology and structure: topographic analysis from a 250-m DEM. Geomorphology 41, 285-307.

30. Kubik, P.W., Christl, M., 2010. $^{10}$Be and $^{26}$Al measurements at the Zurich 6 MV Tandem AMS facility. Nuclear Instruments and Methods in Physics Research Section B- Beam Interactions with Materials and Atoms 268, 880-883.

31. Kubik, P.W., Christl, M., Alfimov, V., 2009. New primary $^{10}$Be standard and t1/2 for AMS at ETH- Recalibration of the in-house $^{10}$Be standards. Laboratory of Ion Beam Physics, Annual Report 2009. ETH Zürich, Zurich, p. 12.

32. Lal, D., 1991. Cosmic ray labeling of erosion surfaces: in situ nuclide production rates and erosion models. Earth Planet. Sci. Lett. 104, 424-439.

33. Lupker, M., Blard, P.-H., Lavé, J., France-Lanord, C., Leanni, L., Puchol, N., Charreau, J., Bourlès, D., 2012. $^{10}$Be-derived Himalayan denudation rates and sediment budgets in the Ganga basin. Earth Planet. Sci. Lett. 333-334, 146-156.

34. Malusà M.G., Balestrieri M.L., 2012. Burial and exhumation across the Alps-Apennines junction zone constrained by fission-track analysis on modern river sands. Terra Nova 24, 221-226.

35. Malusà, M.G., Faccenna, C., Baldwin, S.L., Fitzgerald, P.G., Rossetti, F., Balestrieri, M.L., Danišík, M., Ellero, A., Ottria, G., Piromallo, C., 2015. Contrasting styles of (U)HP rock exhumation along the Cenozoic Adria-Europe plate boundary (Western Alps, Calabria, Corsica). Geochem. Geophys. Geosyst. 16, 1786-1824.

36. Ministero dei Lavori Pubblici, 1960. Consiglio superiore servizio idrografico, scale 1: 100,000, Carta della precipitazione nevosa media annua in Italia nel quarantennio, 1921-1960.

37. Niedermann, S., 2002. Cosmic-Ray-Produced Noble Gases in Terrestrial Rocks: Dating Tools for Surface Processes. Reviews in Mineralogy and Geochemistry 47, 731-784.

630 38. Niedermann, S., Graf, T., Marti, K., 1993. Mass spectrometric identification of cosmic-ray-produced
631 neon in terrestrial rocks with multiple neon components. Earth Planet. Sci. Lett. 118, 65-73.

632 39. Niedermann, S., Bach, W., Erzinger, J., 1997. Noble gas evidence for a lower mantle component in
633 MORBs from the southern East Pacific Rise: Decoupling of helium and neon isotope systematics.
634 Geochim. Cosmochim. Acta 61, 2697-2715.

635 40. Norton, K., von Blanckenburg, F., DiBiase, R., Schlunegger, F., Kubik, P., 2011. Cosmogenic $^{10}$Be-
636 derived denudation rates of the Eastern and Southern European Alps. Int. J. Earth Sci. 100, 1163-
637 1179.

638 41. Phillips, F.M., Argento, D.C., Balco, G., Caffee, M.W., Clem, J., Dunai, T.J., Finkel, R., Goehring, B.,
639 Gosse, J.C., Hudson, A.M., Jull, A.J.T., Kelly, M.A., Kurz, M., Lal, D., Lifton, N., Marrero, S.M.,
640 Nishiizumi, K., Reedy, R.C., Schaefer, J., Stone, J.O.H., Swanson, T., Zreda, M.G., 2016. The CRONUS-
641 Earth Project: A synthesis. Quaternary Geochronology 31, 119-154.

642 42. Schaller, M., von Blanckenburg, F., Veldkamp, A., Tebbens, L.A., Hovius, N., Kubik, P.W., 2002. A 30
643 000 yr record of erosion rates from cosmogenic $^{10}$Be in Middle European river terraces. Earth Planet.
644 Sci. Lett. 204, 307-320.

645 43. Simpson, G., Castelltort, S., 2012. Model shows that rivers transmit high-frequency climate cycles to
646 the sedimentary record. Geology 40, 1131-1134.

647 44. Syvitski, J.P.M., Kettner, A.J., 2007. On the flux of water and sediment into the Northern Adriatic Sea.
648 Cont. Shelf Res. 27, 296-308.

649 45. Ufficio Idrografico e Mareografico di Parma, Bacino del Po, 1984. Annali Idrologici, part II. Istituto
650 Poligrafico della Stato, edited by Cati, L., Roma, Italy.

651 46. Vermeesch, P., Balco, G., Blard, P.-H., Dunai, T.J., Kober, F., Niedermann, S., Shuster, D.L., Strasky, S.,
652 Stuart, F.M., Wieler, R., Zimmermann, L., 2015. Interlaboratory comparison of cosmogenic $^{21}$Ne in
653 quartz. Quat. Geochron. 26, 20-28.

654 47. von Blanckenburg, F., 2005. The control mechanisms of erosion and weathering at basin scale from
655 cosmogenic nuclides in river sediment. Earth Planet. Sci. Lett. 237, 462-479.

656 48. von Blanckenburg, F., Hewawasam, T., Kubik, P.W., 2004. Cosmogenic nuclide evidence for low
657 weathering and denudation in the wet, tropical highlands of Sri Lanka. J. Geophys. Res. Earth Surface
658 109, doi:10.1029/2003JF000049.

659 49. Vörösmarty, C.J., Meybeck, M., Fekete, B., Sharma, K., Green, P., Syvitski, J.P.M., 2003.
660 Anthropogenic sediment retention: Major global impact from registered river impoundments. Global
661 and Planetary Change 39, 169-190.

662 50. Wittmann, H., von Blanckenburg, F., 2009. Cosmogenic nuclide budgeting of floodplain sediment
663 transfer. Geomorphology 109, 246-256.

664 51. Wittmann, H., von Blanckenburg, F., Kruesmann, T., Norton, K.P., Kubik, P.W., 2007. Relation
665 between rock uplift and denudation from cosmogenic nuclides in river sediment in the Central Alps
666 of Switzerland. J. Geophys. Res. Earth Surface 112, F04010, doi: 10.1029/2006JF000729.

667 52. Wittmann, H., von Blanckenburg, F., Guyot, J.L., Maurice, L., Kubik, P.W., 2009. From source to sink:
668 Preserving the cosmogenic $^{10}$Be-derived denudation rate signal of the Bolivian Andes in sediment of
669 the Beni and Mamoré foreland basins. Earth Planet. Sci. Lett. 288, 463-474.

670 53. Wittmann, H., von Blanckenburg, F., Maurice, L., Guyot, J.L., Filizola, N., Kubik, P.W., 2011a. Sediment
671 production and delivery in the Amazon River basin quantified by in situ-produced cosmogenic
672 nuclides and recent river loads. Geol. Soc. Am. Bull. 123, 934-950.

673 54. Wittmann, H., von Blanckenburg, F., Maurice, L., Guyot, J.L., Kubik, P., 2011b. Recycling of Amazon
674 floodplain sediment quantified by cosmogenic $^{26}$Al and $^{10}$Be. Geology 39, 467-470.

675 55. Zanchetta, S., Malusà, M.G., Zanchi, A., 2015. Precollisional development and Cenozoic evolution of
676 the Southalpine retrobelt (European Alps). Lithosphere 7, 662-681.

677

678

679 FIGURES and CAPTIONS

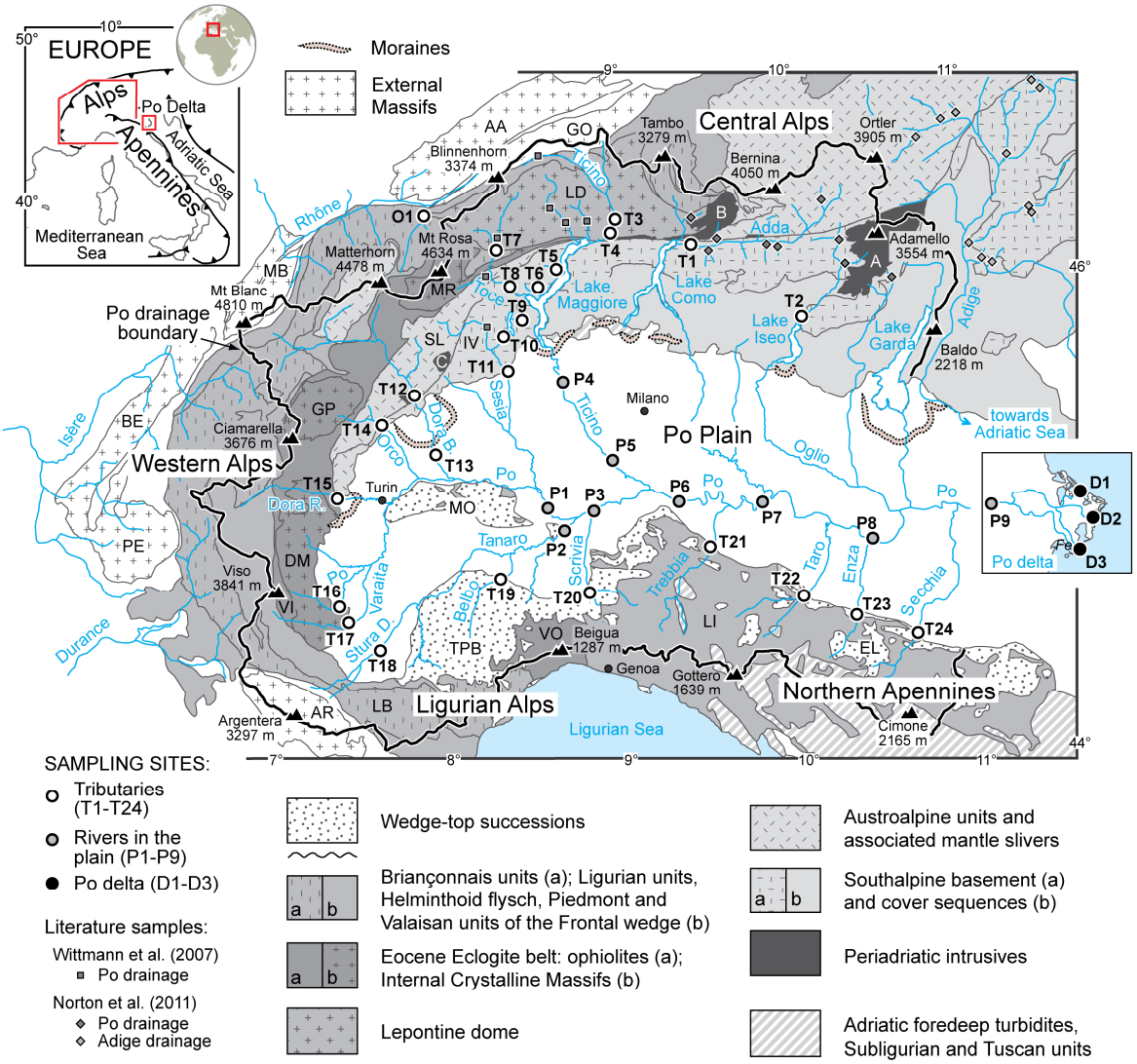


680

681 **Figure 1. Po river drainage with major lakes, moraine amphitheaters, and sampling locations of this work**
682 **and additional literature samples** (Wittmann et al., 2007; Norton et al., 2011). Samples from the Adige
683 catchment are also included. Tectonic units from Malusà et al. (2015), acronyms: A, Adamello; AA, Aar; AR,
684 Argentera; B, Bregaglia-Bergell; BE, Belledonne; C, Biella; DM, Dora-Maira; EL, Epiligurids; GO, Gotthard; GP,
685 Gran Paradiso; IV, Ivrea-Verbano; LB, Ligurian Briançonnais; LD, Lepontine dome; MB, Mont Blanc; MO,
686 Monferrato; MR, Monte Rosa; PE, Pelvoux; SL, Sesia-Lanzo; TPB, Tertiary Piedmont basin; VI, Viso; VO, Voltri.
687 Size: 2 columns

688

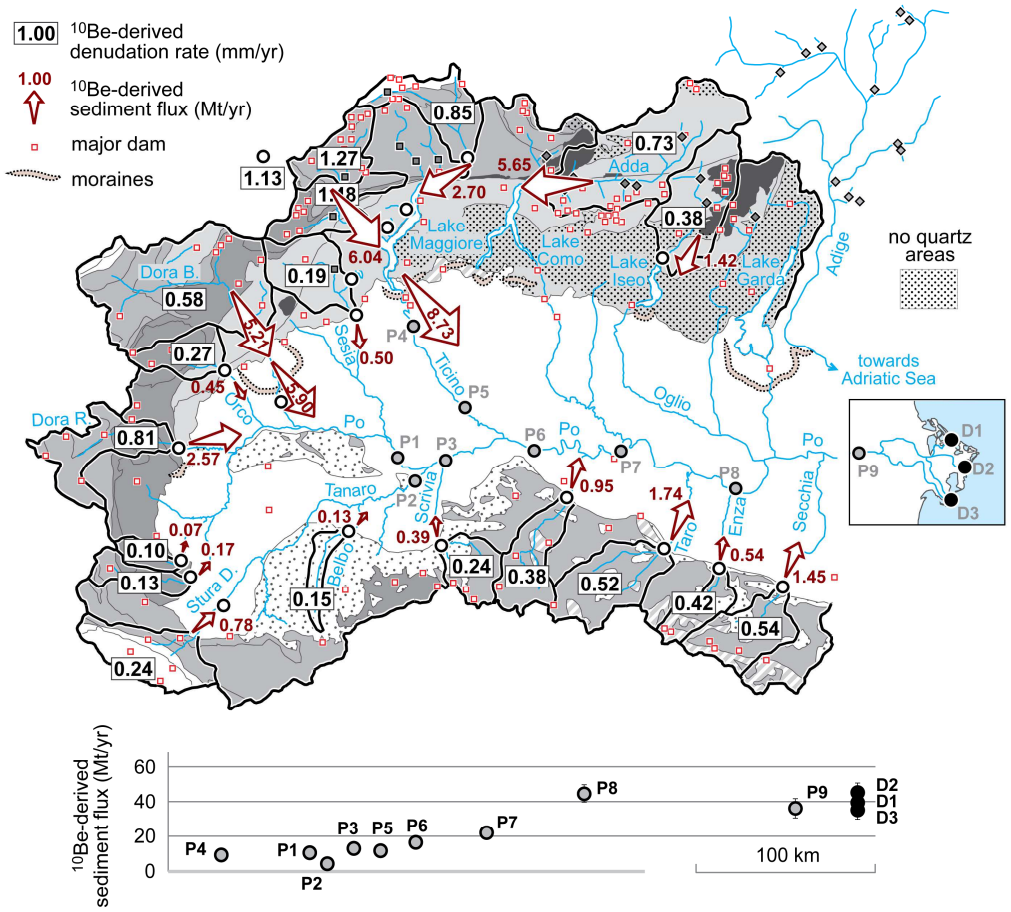


689

690 **Figure 2. Summary of cosmogenic $^{10}$Be-derived denudation rates and sediment fluxes for the source areas**
691 **(upper panel), and floodplain corrected sediment fluxes in the Po Plain (lower panel).** Locations of major
692 dams (height > 15 m, or water volume >$10^6$ $m^3$) after Registro Italiano Dighe
693 (http://www.registroitalianodighe.it/); areas with quartz-free carbonate rocks according to 1:100,000 scale
694 geological maps (http://www.isprambiente.gov.it/it/cartografia); main tectonic units simplified from Fig. 1;
695 other keys as in Fig. 1. In the lower panel, the sediment fluxes downstream of site P7 may be biased towards
696 higher values, because of the basin-wide extrapolation of denudation rates that dominantly reflect the low
697 [$^{10}$Be] values inherited from Apenninic sources.

698 Size: 2 columns

699

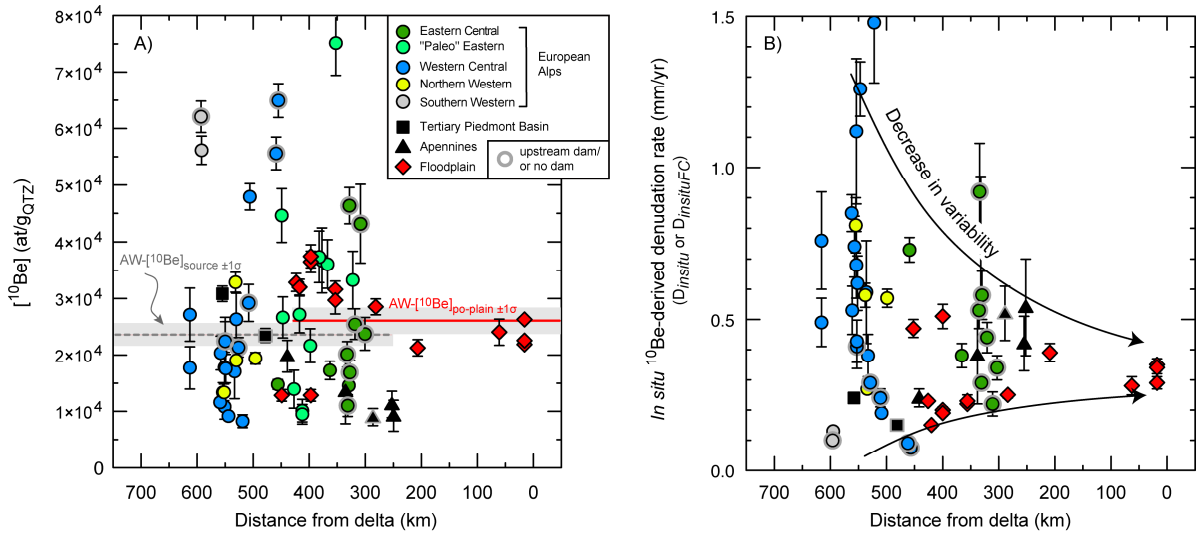


**Figure 3: A- Impact of dams on *in situ* $^{10}$Be concentrations and B- $^{10}$Be-derived denudation rates.** Data (with 1σ error bounds) from this study as well as from Wittmann et al. (2007) and Norton et al. (2011) (Supplement Table S3) are plotted versus distance from the Po delta, and labeled according to the corresponding orogenic segments (samples from the Adige catchment are labeled as "Paleo" Eastern Alps, and sample P2 is added to the Tertiary Piedmont basin group even though it contains ~25% lowland area). Samples from basins without major dams (or collected upstream of the dam) are outlined in blue.. Horizontal lines in A) give area-weighted ("AW") [$^{10}$Be] values (± area-weighted 1σ uncertainties denoted by gray bars) of all Alpine and Apenninic basins upstream of lakes (grey) and area-weighted [$^{10}$Be] of all lowland samples (red). For comparison, the area-weighted [$^{10}$Be] of all basins not influenced by dams is (2.93±0.32)×10$^4$ at/g$_{QTZ}$. Note the strong decrease in variability of denudation rates from source to the floodplain sink in B).

Size: 2 columns

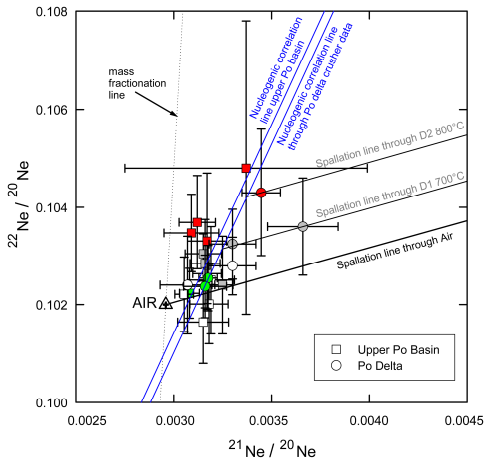


718

719 **Figure 4.** Neon three-isotope diagram showing the stepwise heating (400°C – white, 600-700°C – gray, 800°C
720 – red) and crushing data (green) of six quartz samples from the Po river catchment. An error-weighted fit
721 through all upper Po basin data (squares; see supporting information for details) defines a steep tendency
722 (left blue line), interpreted as the typical signature of nucleogenic Ne of Po basin sediment. Most data from
723 Po delta samples (circles) plot to the right of that line, indicating some addition of cosmogenic Ne to the
724 trapped and nucleogenic components. Therefore, cosmogenic Ne in Po delta samples was calculated
725 assuming a three-component mixture of trapped Ne (as defined by the Po delta crushing data), nucleogenic
726 Ne (steep tendency, right blue line) and cosmogenic Ne ("spallation line" according to Niedermann et al.,
727 1993 shifted through individual data points; gray lines show two examples). The mass fractionation line is
728 shown for reference. Error limits are 2σ .

729 Size: 1.5 columns

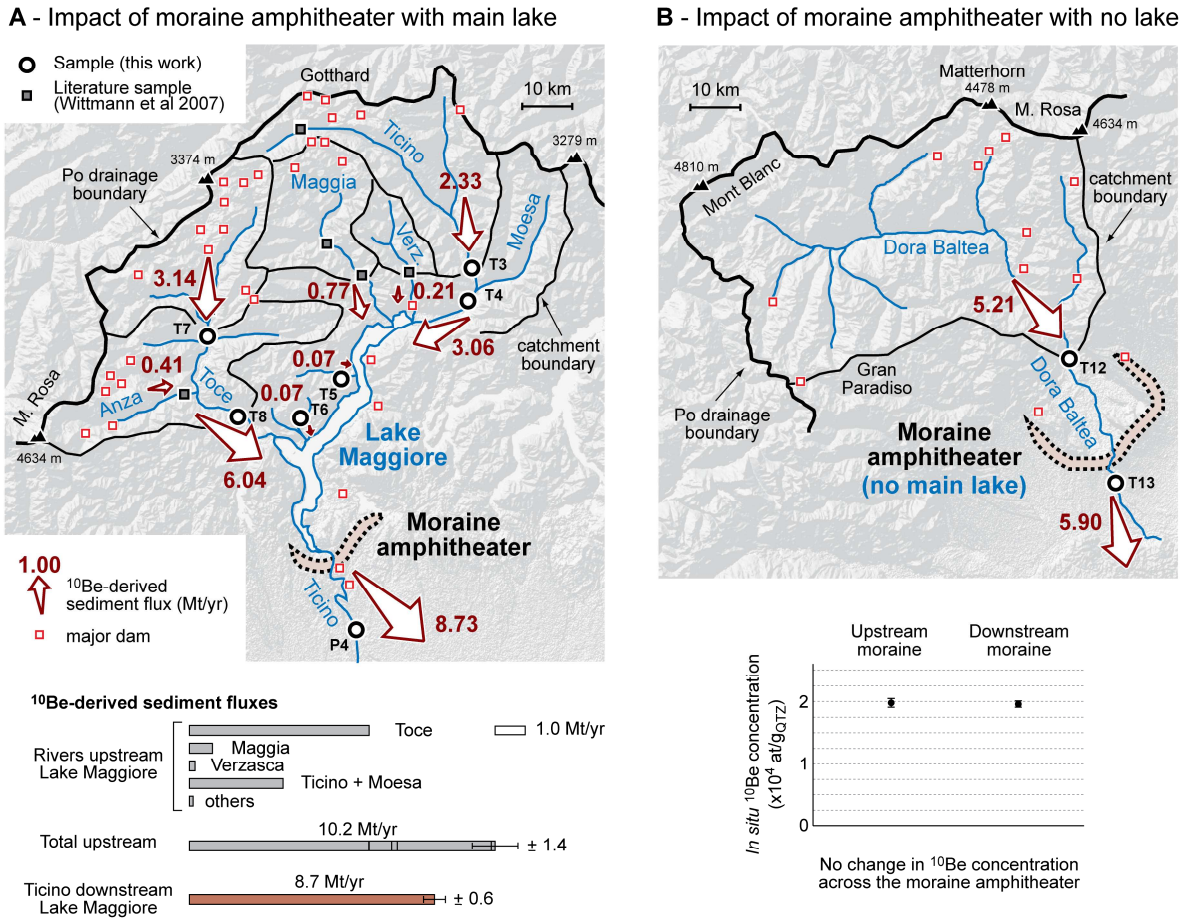


730

731 **Figure 5. Impact of dams, moraines and major lakes on *in situ* $^{10}$Be concentrations and derived sediment**
732 **fluxes in mountain catchments. A (Ticino catchment)**: The sum of $^{10}$Be-derived sediment fluxes in the heavily
733 dammed rivers upstream Lake Maggiore is indistinguishable (within 1σ error) from the $^{10}$Be-derived sediment
734 flux derived from sample P4, collected shortly downstream of the lake (raw data in Tables 1 and S3). **B (Dora**
735 **Baltea catchment)**: The *in situ* [$^{10}$Be] in the sample collected at the exit of the Aosta Valley (T12) is
736 indistinguishable, within 1σ error bounds, from the [$^{10}$Be] in the sample collected shortly downstream of the
737 large moraine amphitheater (T13).
738 Size: 2 columns

739

740

741

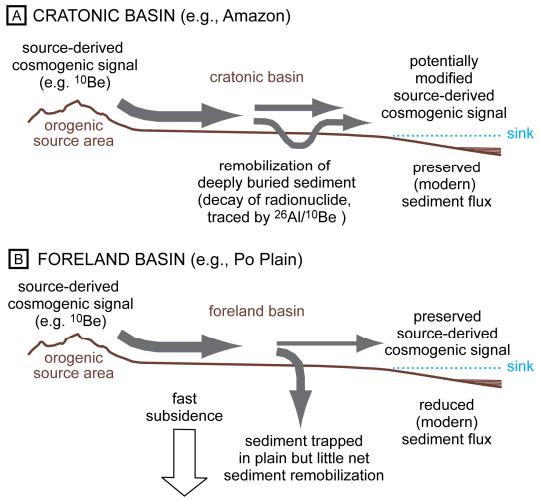


742

743 **Figure 6. The cosmogenic record of mountain erosion in cratonic basins and subsiding foreland basins.** In
744 case A) (cratonic basin), the source-derived $^{10}$Be signal is potentially modified by the addition of deeply buried
745 floodplain material with reduced $^{10}$Be concentrations and $^{26}$Al/$^{10}$Be ratios (Wittmann et al., 2011a, b). In case
746 B) (subsiding foreland basin), the source-derived $^{10}$Be signal is effectively transmitted from the source areas
747 to the sink, as the reworking and export of deeply buried material is limited by subsidence in the floodplain.

748 Size: 1 column

749

750

751

752

753

754

755

**Table 1A: *In situ* $^{10}$Be concentrations, production rates and shielding correction, denudation rate and sediment flux results for mountain basins**

| Short label | River/location | Quartz weight | *In situ* $^{10}$Be concentration | $^{10}$Be amount in blank used for correction | Total, corr. production rate | Total correction factor on production rate[a] | Denudation rate $D_{insitu}$ | Apparent age | Sediment flux $QS_{insitu}$ |
|---|---|---|---|---|---|---|---|---|---|
| | | (g) | (× $10^4$ at/$g_{QTZ}$) | (x $10^4$ at) | (at/$g_{QTZ}$/yr)[a] | | (mm/yr) | (× $10^3$ yr) | (× $10^6$ t/yr)[b] |
| T1 | Adda | 48.27 | 1.480 ± 0.088 | 0.99 | 17.02 | 0.79 | 0.725 ± 0.044 | 0.9 | 5.6 ± 1.8 |
| T2 | Oglio | 49.88 | 1.73 ± 0.16 | 3.48 | 10.03 | 0.61 | 0.380 ± 0.036 | 1.7 | 1.42 ± 0.13 |
| T3 | Ticino, Bellinzona | 40.12 | 1.162 ± 0.075 | 0.99 | 15.64 | 0.81 | 0.853 ± 0.056 | 0.74 | 2.33 ± 0.15 |
| T4 | Ticino, Carasso | 49.96 | 1.34 ± 0.17 | 3.68 | 15.63 | 0.83 | 0.741 ± 0.095 | 0.9 | 3.06 ± 0.39 |
| T5 | Cannobino | 68.95 | 2.14 ± 0.17 | 3.70 | 9.29 | 0.91 | 0.286 ± 0.024 | 2.3 | 0.0651 ± 0.0054 |
| T6 | Bernadino | 48.60 | 2.93 ± 0.33 | 4.11 | 11.03 | 0.89 | 0.244 ± 0.027 | 2.7 | 0.0744 ± 0.0083 |
| T7 | Toce, Masera | 50.76 | 0.916 ± 0.067 | 0.98 | 18.45 | 0.86 | 1.265 ± 0.091 | 0.50 | 3.14 ± 0.22 |
| T8 | Toce, Orvanasso | 61.06 | 0.83 ± 0.11 | 4.10 | 19.58 | 0.91 | 1.48 ± 0.20 | 0.42 | 6.04 ± 0.82 |
| T9 | T. Pesconetto | 44.38 | 5.58 ± 0.29 | 3.70 | 7.02 | 1.00 | 0.0856 ± 0.0045 | 8.0 | 0.00694 ± 0.00036 |
| T10 | Craso del Gallo | 49.12 | 6.52 ± 0.30 | 3.81 | 7.59 | 0.94 | 0.0784 ± 0.0037 | 8.6 | 0.00635 ± 0.00030 |
| T11 | Sesia | 32.52 | 4.81 ± 0.23 | 3.58 | 14.15 | 0.78 | 0.1877 ± 0.0092 | 3.4 | 0.500 ± 0.025 |
| T12 | D. Baltea, Quassolo | 36.24 | 1.99 ± 0.14 | 0.99 | 18.39 | 0.71 | 0.581 ± 0.041 | 1.1 | 5.21 ± 0.37 |
| T13 | D. Baltea, Cigliano | 61.52 | 1.95 ± 0.10 | 3.58 | 17.50 | 0.73 | 0.568 ± 0.030 | 1.1 | 5.90 ± 0.31 |
| T14 | Orco | 51.47 | 3.30 ± 0.18 | 3.47 | 13.72 | 0.70 | 0.266 ± 0.014 | 2.4 | 0.452 ± 0.024 |
| T15 | Dora Riparia | 14.95 | 1.34 ± 0.15 | 0.98 | 17.19 | 0.71 | 0.809 ± 0.087 | 0.78 | 2.57 ± 0.28 |
| T16 | Po, Revello | 41.91 | 6.23 ± 0.28 | 0.99 | 9.91 | 0.71 | 0.1045 ± 0.0047 | 6.3 | 0.0701 ± 0.0031 |
| T17 | Varaita | 39.53 | 5.64 ± 0.25 | 3.54 | 11.65 | 0.82 | 0.1339 ± 0.0060 | 4.8 | 0.1653 ± 0.0074 |
| T18 | Stura Demonte | 45.64 | 3.10 ± 0.14 | 0.98 | 11.50 | 0.69 | 0.241 ± 0.011 | 2.7 | 0.783 ± 0.036 |
| T19 | Belbo | 67.57 | 2.35 ± 0.12 | 0.98 | 5.03 | 0.95 | 0.1523 ± 0.0079 | 4.7 | 0.1349 ± 0.0070 |
| T20 | Scrivia | 23.30 | 1.98 ± 0.28 | 3.52 | 6.89 | 0.90 | 0.237 ± 0.034 | 2.9 | 0.393 ± 0.057 |
| T21 | Trebbia | 6.667 | 1.35 ± 0.57 | 3.53 | 7.76 | 0.91 | 0.38 ± 0.16 | 1.7 | 0.95 ± 0.41 |
| T22 | Taro | 27.30 | 0.90 ± 0.15 | 3.53 | 6.79 | 0.90 | 0.515 ± 0.088 | 1.3 | 1.74 ± 0.30 |
| T23 | Enza | 18.73 | 1.12 ± 0.24 | 3.53 | 6.89 | 0.89 | 0.418 ± 0.090 | 1.6 | 0.54 ± 0.12 |
| T24 | Secchia | 14.66 | 0.92 ± 0.28 | 3.53 | 7.40 | 0.90 | 0.54 ± 0.16 | 1.2 | 1.45 ± 0.44 |
| O1 | Vispa | 120.2 | 1.22 ± 0.14 | 4.20 | 22.12 | 0.64 | 1.13 ± 0.13 | 0.54 | 2.25 ± 0.26 |

[a]Basin-wide pixel-average production rate incl. nucleonic and muonic contributions; given rate is already corrected using total correction factor (encompassing topographic and snow/ice shielding as well as the correction for quartz-free areas). We used the scaling model of Dunai (2000) and a total SLHLproduction rate of 3.75 at/$g_{QTZ}$/yr for calculation.

[b]Calculated using the basin area (in $km^2$) and a sediment density of 2.7 $g/cm^3$.

756

757

**Table 1B: *In situ* $^{10}$Be concentrations, production rates and shielding correction, denudation rate and sediment flux results for lowland samples**

| Short label | River/location | Quartz weight | *In situ* $^{10}$Be concentration | $^{10}$Be amount in blank used for correction | Total, corr. production rate | Total correction factor on production rate[a] | Denudation rate $D_{insitu}$ | Appa-rent age | Floodplain correction[b] | | |
|---|---|---|---|---|---|---|---|---|---|---|---|
| | | | | | | | | | Total, source area production rate | Floodpl.-corr. denudation rate $D_{insituFC}$ | Floodpl.-corr. sediment flux $QS_{insituFC}$ |
| | | (g) | (× $10^4$ at/$g_{QTZ}$) | (x $10^4$ at) | (at/$g_{QTZ}$/yr)[a] | | (mm/yr) | (× $10^3$ yr) | (at/$g_{QTZ}$/yr)[c] | (mm/yr) | (× $10^6$ t/yr) |
| P1 | Po, Valenza | 44.55 | 3.30 ± 0.16 | 0.99 | 10.40 | 0.80 | 0.206 ± 0.010 | 3.2 | 11.8 | 0.230 ± 0.011 | 9.54 ± 0.48 |
| P2 | Tanaro | 48.63 | 3.21 ± 0.14 | 0.99 | 7.07 | 0.85 | 0.1494 ± 0.0066 | 4.5 | 8.12 | 0.1688 ± 0.0074 | 3.71 ± 0.14 |
| P3-1 | Po, Cornale | 35.94 | 3.66 ± 0.19 | 0.99 | 9.12 | 0.85 | 0.1645 ± 0.0085 | 4.0 | 11.05 | 0.196 ± 0.010 | 12.05 ± 0.63 |
| P3-2* | Po, Cornale | 39.35 | 3.76 ± 0.20 | 0.99 | 9.12 | 0.85 | 0.1602 ± 0.0087 | 4.1 | 11.05 | 0.191 ± 0.010 | 11.74 ± 0.64 |
| P4 | Ticino, Vizzola | 62.46 | 1.333 ± 0.089 | 3.58 | 8.11 | 0.68 | 0.463 ± 0.031 | 1.6 | 8.11 | 0.472 ± 0.031 | 8.73 ± 0.58 |
| P5 | Ticino, Bereguardo | 45.44 | 1.29 ± 0.10 | 0.99 | 7.65 | 0.69 | 0.497 ± 0.039 | 1.7 | 8.41 | 0.506 ± 0.041 | 10.20 ± 0.82 |
| P6-1 | Po, Zerbo | 43.19 | 3.18 ± 0.15 | 0.99 | 8.60 | 0.87 | 0.1801 ± 0.0084 | 3.7 | 10.66 | 0.219 ± 0.010 | 17.88 ± 0.82 |
| P6-2* | Po, Zerbo | 25.36 | 2.98 ± 0.25 | 3.53 | 8.60 | 0.87 | 0.192 ± 0.016 | 3.5 | 10.66 | 0.233 ± 0.019 | 19.0 ± 1.6 |
| P7 | Po, Castelnuovo | 61.68 | 2.86 ± 0.14 | 3.58 | 8.56 | 0.84 | 0.1987 ± 0.0097 | 3.3 | 11.11 | 0.252 ± 0.013 | 22.4 ± 1.1 |
| P8 | Po, Viadana | 36.38 | 2.13 ± 0.14 | 3.57 | 9.58 | 0.93 | 0.295 ± 0.020 | 2.2 | 12.8 | 0.385 ± 0.026 | 45.5 ± 3.1 |
| P9 | Po, Crespino | 20.88 | 2.41 ± 0.23 | 3.58 | 8.30 | 0.86 | 0.229 ± 0.022 | 2.9 | 10.45 | 0.283 ± 0.027 | 37.9 ± 3.7 |
| D1 | Po, Boccasette | 17.29 | 2.64 ± 0.17 | 0.99 | 8.28 | 0.86 | 0.209 ± 0.014 | 3.2 | 12.1 | 0.295 ± 0.019 | 41.4 ± 2.7 |
| D2 | Po, Barricata | 30.77 | 2.19 ± 0.12 | 0.95 | 8.28 | 0.86 | 0.252 ± 0.014 | 2.6 | 12.1 | 0.355 ± 0.019 | 49.8 ± 2.6 |
| D3 | Po, Bacucco | 39.42 | 2.26 ± 0.14 | 3.53 | 8.28 | 0.86 | 0.244 ± 0.016 | 2.7 | 12.1 | 0.344 ± 0.021 | 34.2 ± 3.0 |

[a]Basin-wide pixel-average production rate incl. nucleonic and muonic contributions; given rate is already corrected using total correction factor (encompassing topographic and snow/ice shielding as well as the correction for quartz-free areas). We used the scaling model of Dunai (2000) and a total SLHL production rate of 3.75 at/$g_{QTZ}$/yr for calculation.

[b]Floodplain correction carried out using the low-relief elevations determined when having a standard deviation in elevation of <25 m within an area of 15x15 pixels (90 m DEM). Floodpl.-corr. sediment fluxes were calculated using the floodpl.-corr. denudation rate, the source area (Supplement Table S1) and a sediment density of 2.7 g/cm$^3$.

[c]Total production rate for floodplain areas, also corrected using total correction factor.

*Lab replicates processed 6 months later (by dissolving newly weighted material).

758

759

760

761

**Table 2: Stable and cosmogenic Al determinations and estimated cosmogenic $^{21}$Ne excesses**

| Short label | $^{26}$Al/$^{27}$Al AMS ratio ($\times 10^{-13}$)[a] | Stable $^{27}$Al concentration ($\times 10^{-6}$ g/g$_{QTZ}$)[b] | Cosmogenic $^{26}$Al concentration ($\times 10^{4}$ at/g$_{QTZ}$) | Ratio of $^{26}$Al/$^{10}$Be | Cosmogenic $^{21}$Ne excess[c] ($\times 10^{6}$ at/g$_{QTZ}$) |
|---|---|---|---|---|---|
| T15 | 0.99 ± 0.12 | 43.2 ± 1.3 | 9.0 ± 1.1 | 6.7 ± 1.1 | |
| T16 | 4.34 ± 0.26 | 36.9 ± 1.1 | 35.6 ± 2.4 | 5.71 ± 0.46 | |
| T17 | 0.678 ± 0.064 | 227.3 ± 6.8 | 34.3 ± 3.4 | 6.08 ± 0.66 | |
| T18 | 0.60 ± 0.11 | 140.3 ± 4.2 | 18.6 ± 3.4 | 6.0 ± 1.1 | |
| T23 | 0.76 ± 0.18 | 112.0 ± 3.4 | 18.5 ± 4.4 | 16.5 ± 5.3 | |
| T24 | 0.258 ± 0.047 | 166.6 ± 5.0 | 9.1 ± 1.7 | 9.9 ± 3.5 | |
| P1 | 1.62 ± 0.16 | 56.4 ± 1.7 | 20.2 ± 2.1 | 6.13 ± 0.70 | |
| P2 | 0.692 ± 0.096 | 132 ± 4.0 | 20.3 ± 2.9 | 6.32 ± 0.94 | |
| P3-1 | 1.10 ± 0.12 | 97.2 ± 2.9 | 23.6 ± 2.7 | 6.44 ± 0.81 | |
| P6-2* | 0.44 ± 0.052 | 179.6 ± 5.4 | 17.4 ± 2.1 | 5.84 ± 0.86 | |
| D1 | 0.287 ± 0.078 | 375 ± 11 | 23.6 ± 6.5 | 8.9 ± 2.5 | 1.56 (+0.75/-0.68) |
| D2 | 0.1290 ± 0.0049 | 466 ± 14 | 13.19 ± 0.64 | 5.97 ± 0.42 | 0.7 (+1.5/-0.6) |
| D3 | 0.49 ± 0.12 | 121.5 ± 3.6 | 13.2 ± 3.2 | 5.8 ± 1.4 | |

[a]Accelerator mass spectrometer (AMS) ratio; Al analyses were done on the same sample as $^{10}$Be (i.e. the samequartz weight applies). An avg. blank $^{26}$Al/$^{27}$Al ratio of $0.065\times10^{-13}$ (n = 3) was used for blank correction.

[b]An analytical uncertainty of 3%, being the long-term reproducibility, was propagated. No Al spike was added to samples.

[c]Calculation method and detailed noble gas data are presented in supplementary information (Text S2 and Table S3, respectively). Note that for Neon error calculation, 2σ error bounds were used.

*Lab replicate processed 6 months later.

762

763

**Table 3: Modern erosion rates and respective sediment fluxes $QS_M$ and comparison with cosmogenic nuclide-derived sediment fluxes $QS_{insituFC}$**

| | | | | Data taken from reference | | | Calculations from this study | | | |
|---|---|---|---|---|---|---|---|---|---|---|
| **Item** | **River/Station[a]** | **Region** | **Nearest $^{10}$Be sample (km)[b]** | **Drainage area corr. for dams ($km^2$)[c]** | **Obser-vation period (years)** | **"Dam-corr." erosion rate (mm/yr)[d]** | **Surface area at nearest $^{10}$Be sampling point ($km^2$)** | **$QS_M$, re-calcuated using total area upstream of sampling point (× $10^6$ t/yr)[e]** | **Mean $QS_{insitu}$ or $QS_{insituFC}$ (× $10^6$ t/yr)** | **$QS_{C/M}$ (Ratio of $QS_{insituFC}$ to $QS_M$)** |
| 1 | Adda at Tirano | Eastern Central Alps | 65 km upstr. of T1 | 906 | 6 | 0.085 | 2883 | 0.66 | 5.65 | 8.6 |
| 2 | Ticino at Bellinzona/Carasso[f] | Western Central Alps | T3 | *1515* | 28 | 0.20 | 1530 | 0.83 | 3.10 | 3.7 |
| 3 | Maggia at Locarno[f] | Western Central Alps | Mag11-2 & Mag11-4[g] | *926* | 5 | 0.14 | 544 | 0.21 | 0.67[g] | 3.2 |
| 4 | Sesia at Vercelli | Central Alps/Floodplain | 35 km downstr. of T11 | 1706 | 4 | 0.034 | 987 | 0.090 | 0.50 | 5.6 |
| 5-1 | Dora Baltea at Tavagnasco | Northern Western Alps | T12 | 3209 | 10 | 0.27 | 3321 | 2.42 | 5.90 | 2.0 |
| 5-2 | Dora Baltea ("Mountain bas.")[h] | Northern Western Alps | T12 | *3264* | ? | - | 3264 | 1.02 | 5.90 | 4.9 |
| 7 | Tanaro at Montecastello | Ligurian Alps/TPB | P2 | 7985 | 16 | 0.11 | 8145 | 2.38 | 3.71 | 1.6 |
| 8 | Scrivia at Serravalle | Apennines | T20 | 605 | 5 | 0.036 | 614 | 0.060 | 0.39 | 6.5 |
| 9 | Trebbia at S. Salvatore | Apennines | T21 | 631 | 5 | 0.12 | 918 | 0.29 | 0.95 | 3.3 |
| 10 | Taro at Ostia | Apennines | T22 | 408 | 5 | 0.11 | 1248 | 0.37 | 1.74 | 4.7 |
| 11 | Enza at Sorbolo | Apennines | 30 km downstr. of T23 | 670 | 17 | 0.89 | 481 | 1.16 | 0.54 | 0.47 |
| 12 | Secchia at Castellarano | Apennines | T24 | 941 | 5 | 0.41 | 992 | 1.09 | 1.45 | 1.3 |
| 13-1 | Po at Casale Monf. | Floodplain | 20 km upstr. of P1 | *13940* | 10 | 0.019 | 14240[i] | 0.73 | 9.5 | 13.1[k] |
| 13-2 | Po at Becca (Bridge) | Floodplain | 30 km downstr. of P3 | *24730* | 14 | 0.043 | 27520 | 3.20 | 11.9 | 3.7 |
| 13-3 | Po at Piacenza[j] | Floodplain | 20 km upstr. of P7 | *42030* | 24 | - | - | 3.32[j] | 22.4 | 6.7 |
| 13-4 | Po at Boretto[j] | Floodplain | P8 | *55183* | 23 | - | - | 9.71[j] | 45.5 | 4.7 |
| 13-5 | Po at Pontelagoscuro[j] | Floodplain | 25 km upstr. of P9 | *70091* | 24 | - | - | 11.4[j] | 37.9 | 3.3 |

[a]Data mainly from Bartolini et al. (1996), who measured suspended sediment only; if not noted otherwise, the measurement station is reasonably close to a cosmogenic nuclide sampling point.

[b]Distance to nearest $^{10}$Be sampling point (in km) or sampling point in direct vicinity.

[c]"Area where erosion actually occurs" (from Bartolini et al., 1996, if not indicated otherwise). Numbers in italics give total basin area upstream of this point, which was then also used for calculations.

[d]From susp. load measurements assuming a bedrock density of 2700 kg/m$^3$; erosion rate calc. using the drainage area corr. for dam influence (only for data by Bartolini et al., 1996).

[e]Calc. using a bedrock density of 2700 kg/m$^3$ and surface area "at nearest cosmo sampling point". Note that for lowland basins, this is the "source area" (see Table S1).

[f]Data from Table 1 in Hinderer et al. (2013) where original reference can be found. Note that for the Ticino and the Po at the delta, dissolved loads are included in estimated "erosion rate", and all items taken from Hinderer et al. (2013) also include a bedload estimate (that is notably 0% in the lower Po according to original references).

[g]Data from Wittmann et al. (2007), see supplementary data Tables S1, S2.

[h]From Autorità di Bacino del Fiume Po (2001).

[i]Area excluding the Sesia drainage basin (to enable comparison with surface area at P1).

[j]Data from Ufficio Idrografico e Mareografico di Parma (1984), where mean sediment loads are reported (and not denudation rates and thus a recalculation using surface area is not necessary).

[k]Datapoint excluded from the discussion in section 6.3.

765